

Министерство науки и высшего образования Российской Федерации
ФЕДЕРАЛЬНОЕ ГОСУДАРСТВЕННОЕ АВТОНОМНОЕ ОБРАЗОВАТЕЛЬНОЕ
УЧРЕЖДЕНИЕ ВЫСШЕГО ОБРАЗОВАНИЯ
НАЦИОНАЛЬНЫЙ ИССЛЕДОВАТЕЛЬСКИЙ УНИВЕРСИТЕТ ИТМО
ITMO University

ВЫПУСКНАЯ КВАЛИФИКАЦИОННАЯ РАБОТА
GRADUATION THESIS

Субизлучательные двухчастичные возбуждения в ансамблях квантовых эмиттеров /
Doubly Excited Subradiant States in Ensembles of Quantum Emitters

Обучающийся / Student Устименко Никита Алексеевич

Факультет/институт/кластер/ Faculty/Institute/Cluster физический факультет

Группа/Group Z42761

Направление подготовки/ Subject area 12.04.03 Фотоника и оптоинформатика

Образовательная программа / Educational program Техническая физика / Physics and engineering 2021

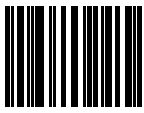
Язык реализации ОП / Language of the educational program Русский, Английский

Статус ОП / Status of educational program МОП

Квалификация/ Degree level Магистр

Руководитель ВКР/ Thesis supervisor Петров Михаил Игоревич, PhD, физико-математические науки, Университет ИТМО, физический факультет, старший научный сотрудник

Обучающийся/Student

Документ подписан	
Устименко Никита Алексеевич	
24.05.2023	

(эл. подпись/ signature)

Устименко
Никита
Алексеевич

(Фамилия И.О./ name
and surname)

Руководитель ВКР/
Thesis supervisor

Документ подписан	
Петров Михаил Игоревич	
24.05.2023	

(эл. подпись/ signature)

Петров Михаил
Игоревич

(Фамилия И.О./ name
and surname)

**Министерство науки и высшего образования Российской Федерации
ФЕДЕРАЛЬНОЕ ГОСУДАРСТВЕННОЕ АВТОНОМНОЕ ОБРАЗОВАТЕЛЬНОЕ
УЧРЕЖДЕНИЕ ВЫСШЕГО ОБРАЗОВАНИЯ
НАЦИОНАЛЬНЫЙ ИССЛЕДОВАТЕЛЬСКИЙ УНИВЕРСИТЕТ ИТМО
ITMO University**

**ЗАДАНИЕ НА ВЫПУСКНУЮ КВАЛИФИКАЦИОННУЮ РАБОТУ /
OBJECTIVES FOR A GRADUATION THESIS**

Обучающийся / Student Устименко Никита Алексеевич
Факультет/институт/кластер/ Faculty/Institute/Cluster физический факультет
Группа/Group Z42761
Направление подготовки/ Subject area 12.04.03 Фотоника и оптоинформатика
Образовательная программа / Educational program Техническая физика / Physics and engineering 2021
Язык реализации ОП / Language of the educational program Русский, Английский
Статус ОП / Status of educational program МОП
Квалификация/ Degree level Магистр
Тема ВКР/ Thesis topic Субизлучательные двухчастичные возбуждения в ансамблях квантовых эмиттеров / Doubly excited subradiant states in ensembles of quantum emitters
Руководитель ВКР/ Thesis supervisor Петров Михаил Игоревич, PhD, физико-математические науки, Университет ИТМО, физический факультет, старший научный сотрудник

Основные вопросы, подлежащие разработке / Key issues to be analyzed

Goal and tasks of the project:

Goal: investigation and development of subradiant doubly excited states in small ensembles of quantum emitters

Tasks:

1. Analytical description of singly and doubly excited eigenstates of ring ensembles.
2. Investigation of the mechanism of two-mode interaction for the suppression of one- and two-photon emission of collective states.
3. Numerical modeling of singly and doubly excited eigenstates. Optimization of two-photon emission rate.
4. Simulation of two-photon amplitude in the far-field regime.

Content of the thesis (list of key issues to be analyzed):

1. Introduction
2. Theoretical description of ensembles of quantum emitters.
 - 2.1. Effective Hamiltonian of dipole-dipole interaction in free space.
 - 2.2. Singly and doubly excited collective states. Derivation of the effective Schrodinger equations from the Lindblad equation.
3. Eigenstates of a single ring of emitters
 - 3.1. Singly excited eigenstates and eigenenergies.
 - 3.2. Projection of quasi-angular momentum of the state.
 - 3.3. Doubly excited eigenstates. Relation with the singly excited states.
 - 3.4. Collective emission rates of a small single ring.
4. Subradiant eigenstates of ring ensembles.

- 4.1. Mechanism of subradiance for small ensembles: two-mode interaction.
 - 4.2. An example of $m = 0$.
 - 4.3. Scattering of Bessel beam by ring ensemble.
 - 4.3. Eigenvalue equation for singly excited states in multi-ring structure.
 - 4.4. Subradiant states with the non-zeroth projection of quasi-angular momentum.
 - 4.5. Far-field radiation patterns. Multipolar expansion.
 - 4.6. Doubly excited subradiant states.
 - 4.7. Far-field two-photon amplitude.
- Conclusion.

Recommended materials and sourcebooks for completion of thesis:

Reitz M., Sommer C., Genes C. Cooperative quantum phenomena in light-matter platforms //PRX Quantum. – 2022. – Vol. 3. – №. 1. – p. 010201.

Solntsev A. S., Agarwal G. S., Kivshar Y. S. Metasurfaces for quantum photonics //Nature Photonics. – 2021. – Vol. 15. – №. 5. – p. 327-336.

Asenjo-Garcia A. et al. Exponential improvement in photon storage fidelities using subradiance and “selective radiance” in atomic arrays //Physical Review X. – 2017. – Vol. 7. – №. 3. – p. 031024.

Cremer J. et al. Polarization control of radiation and energy flow in dipole-coupled nanorings //New Journal of Physics. – 2020. – Vol. 22. – №. 8. – p. 083052.

Kornovan D. F. et al. High-Q localized states in finite arrays of subwavelength resonators //ACS Photonics. – 2021. – Vol. 8. – №. 12. – p. 3627-3632.

Дата выдачи задания / Assignment issued on: 15.01.2023

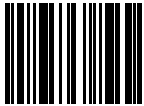
Срок представления готовой ВКР / Deadline for final edition of the thesis 20.05.2023

Характеристика темы ВКР / Description of thesis subject (topic)

Тема в области фундаментальных исследований / Subject of fundamental research: да / yes

СОГЛАСОВАНО / AGREED:

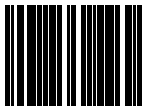
Руководитель ВКР/
Thesis supervisor

Документ подписан	
Петров Михаил Игоревич	
10.03.2023	

Петров Михаил
Игоревич

(эл. подпись)

Задание принял к
исполнению/ Objectives
assumed BY

Документ подписан	
Устименко Никита Алексеевич	
17.03.2023	

Устименко
Никита
Алексеевич

(эл. подпись)

Руководитель ОП/ Head
of educational program

Документ подписан	
Белов Павел Александрович	
24.05.2023	

Белов Павел
Александрович

(эл. подпись)

**Министерство науки и высшего образования Российской Федерации
ФЕДЕРАЛЬНОЕ ГОСУДАРСТВЕННОЕ АВТОНОМНОЕ ОБРАЗОВАТЕЛЬНОЕ
УЧРЕЖДЕНИЕ ВЫСШЕГО ОБРАЗОВАНИЯ
НАЦИОНАЛЬНЫЙ ИССЛЕДОВАТЕЛЬСКИЙ УНИВЕРСИТЕТ ИТМО
ITMO University**

**АННОТАЦИЯ
ВЫПУСКНОЙ КВАЛИФИКАЦИОННОЙ РАБОТЫ
SUMMARY OF A GRADUATION THESIS**

Обучающийся / Student Устименко Никита Алексеевич

Факультет/институт/кластер/ Faculty/Institute/Cluster физический факультет

Группа/Group Z42761

Направление подготовки/ Subject area 12.04.03 Фотоника и оптоинформатика

Образовательная программа / Educational program Техническая физика / Physics and engineering 2021

Язык реализации ОП / Language of the educational program Русский, Английский

Статус ОП / Status of educational program МОП

Квалификация/ Degree level Магистр

Тема ВКР/ Thesis topic Субизлучательные двухчастичные возбуждения в ансамблях квантовых эмиттеров / Doubly Excited Subradiant States in Ensembles of Quantum Emitters

Руководитель ВКР/ Thesis supervisor Петров Михаил Игоревич, PhD, физико-математические науки, Университет ИТМО, физический факультет, старший научный сотрудник

**ХАРАКТЕРИСТИКА ВЫПУСКНОЙ КВАЛИФИКАЦИОННОЙ РАБОТЫ
DESCRIPTION OF THE GRADUATION THESIS**

Цель исследования / Research goal

Развитие субизлучательных (высокодобротных) одно- и двухчастичных возбуждений с угловым моментом в ансамблях двухуровневых эмиттеров \ Development of singly and doubly excited subradiant (high-Q) eigenstates with angular momentum in ensembles of two-level emitters

Задачи, решаемые в ВКР / Research tasks

1) Развить теоретический анализ собственных состояний олигомеров с симметрией относительно поворота в плоскости на основе эффективного уравнения Шредингера и теории групп; 2) исследование одночастичных высокодобротных возбуждений с угловым моментом и механизма их формирования; 3) исследование двухчастичных высокодобротных возбуждений и их связь с одночастичными высокодобротными возбуждениями, включая правила отбора. \ 1) Develop theoretical analysis of eigenstates in oligomers with in-plane rotational symmetry based on effective Schrodinger equation and group theory; 2) investigation of singly excited high-Q states with angular momentum and mechanism of their formation; 3) investigation of doubly excited high-Q states and their mapping to singly excited high-Q states including selection rules.

Краткая характеристика полученных результатов / Short summary of results/findings

В работе исследуются субизлучательные (высокодобротные) одночастичные (ОЧ) и двухчастичные (ДЧ) возбуждения с угловым моментом (m) в ансамблях двухуровневых

дипольных эмиттеров, которые могут хранить возбуждения в виде когерентных коллективных состояний. 1) Проведен теоретический анализ собственных состояний в структурах эмиттеров с симметрией относительно поворота в плоскости, в которых возбуждения обладают угловым моментом. Во-первых, сформулированы эффективные уравнения, позволяющие находить ОЧ и ДЧ собственные состояния с разными угловыми моментами в системе концентрических колец эмиттеров. Во-вторых, выведено количество ДЧ собственных состояний с различным угловым моментом в таких системах. В-третьих, сформулировано правило отбора вкладов произведений ОЧ состояний в ДЧ состояние: неприводимое представление ДЧ состояния должно входить в произведение неприводимых представлений ОЧ состояний. 2) Для получения субизлучательных состояний берутся олигомеры, которые можно рассматривать как две подсистемы излучателей. Взаимодействие между состояниями подсистем, обладающими одинаковой симметрией, приводит к образованию симметричных и антисимметричных состояний, которые обладают симметрией исходных состояний. Показано, что из-за деструктивной интерференции между подсистемами антисимметричное состояние имеет добротность много больше, чем добротность одиночного излучателя, при расстояниях между излучателями менее четверти резонансной длины волны одиночного эмиттера. В частности, кольцо с эмиттером в центре поддерживает высокодобротное ОЧ возбуждение с $m = 0$, тогда как два кольца поддерживают высокодобротные ОЧ возбуждения со всеми значениями m . 3) Два кольца поддерживают 66 двухчастичных возбуждения, из которых десять имеют $m = 3$. Самым высокодобротным ДЧ возбуждением является возбуждение с $m = 3$, которое представляет собой пару высокодобротных ОЧ возбуждений с $m = 1$ и $m = 2$, а энергия этого ДЧ возбуждения с $m = 3$ является суммой энергий высокодобротных ОЧ возбуждений с $m = 1$ и $m = 2$.

This thesis investigates subradiant (high-Q) singly excited (SE) and doubly excited (DE) states with angular momentum (m) in ensembles of two-level dipole emitters that can store the excitations in coherent collective states. 1) Theoretical analysis of eigenstates in structures of emitters with in-plane rotational symmetry is performed. Excitations in such structures can have angular momentum. Firstly, we formulated the effective equations that allow us to find SE and DE eigenstates with different angular momentum in the system of concentric rings of emitters. Secondly, the number of DE eigenstates with different angular momentum in such systems is derived. Thirdly, the selection rule for contributions of products of SE states into a DE state is formulated: the irreducible representation of the DE state should enter the product of irreducible representations of SE states. 2) To achieve subradiant states, we consider oligomers that can be viewed as comprising two subsystems of emitters. The interaction between subsystems' states possessing the same symmetry results in the formation of symmetric and anti-symmetric states, which also retain the initial states' symmetry. It is shown that, due to destructive interference between subsystems, the anti-symmetric state has a large Q-factor compared to that of a single emitter for separations between emitters smaller than a quarter of the emitter's resonant wavelength. In particular, a ring with a central emitter maintains a high-Q SE state with $m = 0$, whereas two rings maintain high-Q SE states with all values of m . 3) Two rings maintain 66 excited eigenstates, and ten of them have $m = 3$. The most subradiant DE state is the state with $m = 3$ which is a pair of excitations with $m = 1$ and $m = 2$ in high-Q SE states. The energy of this DE state with $m = 3$ is a sum of energies of high-Q SE states with $m = 1$ and $m = 2$.

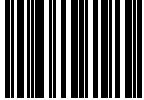
Наличие публикаций по теме выпускной работы / Publications on the topic of the thesis

1. Устименко Н.А., Волков И.А., Корнован Д.Ф., Савельев Р.С., Шеремет А.С., Петров М.И. Субрадиационные однофотонные и двухфотонные состояния в двумерных ансамблях квантовых излучателей//Енисейская Фотоника – 2022. Всероссийская научная конференция с международным участием. Тезисы докладов - 2022. - Т. 2. - С. 92-93 (Тезисы)

Наличие выступлений на конференциях по теме выпускной работы / Conference reports on the topic of the thesis

1. XII Конгресс молодых ученых ИТМО, 03.04.2023 - 06.04.2023 (Конференция, статус - всероссийский)
2. Всероссийская научная конференция с международным участием «ЕНИСЕЙСКАЯ ФОТОНИКА – 2022», 19.09.2022 - 24.09.2022 (Конференция, статус - международный)

Обучающийся/Student

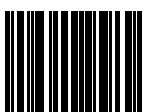
Документ подписан	
Устименко Никита Алексеевич	
24.05.2023	

(эл. подпись/ signature)

Устименко
Никита
Алексеевич

(Фамилия И.О./ name
and surname)

Руководитель ВКР/
Thesis supervisor

Документ подписан	
Петров Михаил Игоревич	
24.05.2023	

(эл. подпись/ signature)

Петров Михаил
Игоревич

(Фамилия И.О./ name
and surname)

CONTENTS

INTRODUCTION	9
1 THEORETICAL DESCRIPTION OF QUANTUM EMITTER ENSEMBLES	14
1.1 Effective Hamiltonian and spontaneous emission of radiation	14
1.2 Effective Schrödinger equation	18
1.3 Singly and doubly excited collective states	19
1.4 Green's tensor in free space	21
2 EIGENSTATES OF A SINGLE RING AND MULTIRING ENSEMBLES OF EMITTERS	24
2.1 The single excitation spectrum of a ring. Angular quasi-momentum	24
2.2 Relation between angular quasi-momentum and irreducible representation	27
2.3 Selection rules for expansions of doubly excited states	30
2.4 Remark on the numerical calculation of degenerate eigenstates	32
2.5 The single excitation spectrum of a multi-ring structure	32
2.6 Doubly excited eigenstates	34
3 SUBRADIANT EIGENSTATES OF RING OLIGOMERS	41
3.1 Subradiance of a small single ring	41
3.2 Mechanism of subradiant state formation	44
3.3 An example of $m = 0$ with a central emitter	45
3.4 Subradiant states with non-zero angular quasi-momentum	47
3.5 Doubly excited subradiant states	51
3.6 Far-field radiation patterns of singly excited states	56
3.7 Multipole expansion	58
3.8 Far-field two-photon amplitude	62
CONCLUSION	65
REFERENCES	67

INTRODUCTION

Artificial ensembles of ordered two-level systems – quantum emitters – support collective excitations stored in coherent collective states of dipole-coupled emitters. Such ensembles can significantly enhance light-matter interaction and photon storage at the nanoscale [1, 2] which has a great potential for various quantum applications including metrology [3], memory [4], and computations [5]. However, in free space, the coupling strength between dipole emitters is small relative to the transition energy of a single emitter ($\hbar\omega_0$), and such a coupling regime is known in the literature as a weak coupling [6]. In the weak coupling regime, the collective states of atoms, free from absorption due to non-radiative losses, are susceptible to a decoherence mechanism due to spontaneous emission governed by the decay rate of the state γ . It has been shown that the proper management of the emitter arrangement allows reaching $\gamma \ll \gamma_0$ associated with a subradiant eigenstate in the ensemble where γ_0 is the decay rate of a single emitter (its natural linewidth, or inverse lifetime).

The interest in subradiant states with large lifetime originates from the classical work of Robert Dicke [7]. In this work, R. Dicke showed that constructive interference between atoms leads to a significant increase in their radiation, which is known as the superradiance effect. However, R. Dicke also considered the opposite effect of destructive interference for a dimer of identical two-level systems which cannot radiate being in an anti-symmetric (subradiant) state with one excitation. Thus, the collective spontaneous emission of an atomic ensemble can be significantly suppressed due to destructive interference in a light-mediated inter-atomic interaction, and the lifetime of stored excitations can be increased. This effect is known as the subradiance. For a long time, this effect remained a theoretical concept [8, 9, 10] until it was experimentally demonstrated for a pair of trapped ions [11] and later for molecules [12] and atomic clouds [13].

A further increase in the lifetimes of atomic systems became possible due to the ordering of atoms into structures of various geometries. Thanks to the active development of manipulation methods in atomic optics and nano-optomechanics in recent years, it has become possible to arrange ultracold atoms and other quantum emitters by optical traps into ordered 1D [14], 2D [15, 16], or 3D [17] structures at near-zero temperature. The subradiant states with one and two excitations

have been reported for periodic one-dimensional chains in free space and near a waveguide [2, 18, 19, 20, 21, 22, 23], and in two-dimensional arrays [3, 24, 25].

Since the radiation leakage in chains and lattices is primarily from open boundaries, we investigate in this thesis subradiant states of closed ensembles such as rings of quantum emitters in free space. The main feature of eigenstates in rings is a well-defined integer angular quasi-momentum. To the best of our knowledge, H. S. Freedhoff for the first time analyzed the radiative properties of singly excited states of a single ring when N emitters are placed at the N vertices of a regular polygon for $N = 3$ in Ref. [26], and $N \leq 6$ in Ref. [27]. In Ref. [25], A. Asenjo-Garcia et al. reported that the lifetime of singly excited eigenstates of a single ring for a fixed separation between the emitters grows exponentially with N similar to whispering gallery modes of disk resonators [28]. In Ref. [29], J. Cremer et al. found a polynomial scaling with N of the most subradiant doubly excited state for a fixed separation between emitters. The reported singly excited subradiant states have been applied to efficiently transfer an excitation between two rings placed in one plane [25, 29], to develop a nano-antenna, [30] and a thresholdless laser [31]. In Ref. [32], H.H. Jen et al. studied the scattering of optical beams with different angular momentum on atomic rings and demonstrated remarkable differences in their radiation patterns.

As shown in Ref. [33] by M. Moreno-Cardoner et al., the lifetime of the most long-lived state in a single ring becomes larger than the lifetime of the most long-lived state in a linear chain with the same parameters only for a quite large number of emitters $N \gtrsim 40$. Therefore, it motivates us to develop mechanisms of radiative loss suppression for states with angular momentum available for relatively small ensembles $N \lesssim 10$ – oligomers – with a focus on underexamined doubly excited states. In this thesis, we suggest a mechanism inspired by the Friedrich-Wintgen mechanism for two resonant systems (or resonant modes) coupled via free propagating photons (radiation continuum) [34]. This mechanism explains the formation of high-Q states in optical resonators or their arrays, including rings, known as quasi-bound states in the continuum [35, 36, 37].

Thus, this thesis is devoted to the development of singly and doubly excited subradiant eigenstates in oligomers of two-level dipole emitters in free space [see figure 1(a)]. The oligomers have in-plane rotational symmetry, therefore, their eigenstates have angular quasi-momentum. The **first chapter** presents

Schrödinger equation with an effective, non-Hermitian Hamiltonian that should be solved in order to find the eigenstates of the ensemble. In this formalism, the coupling between emitters is governed by the classical electromagnetic Green's tensor at the resonant frequency ω_0 depending only on the positions of emitters.

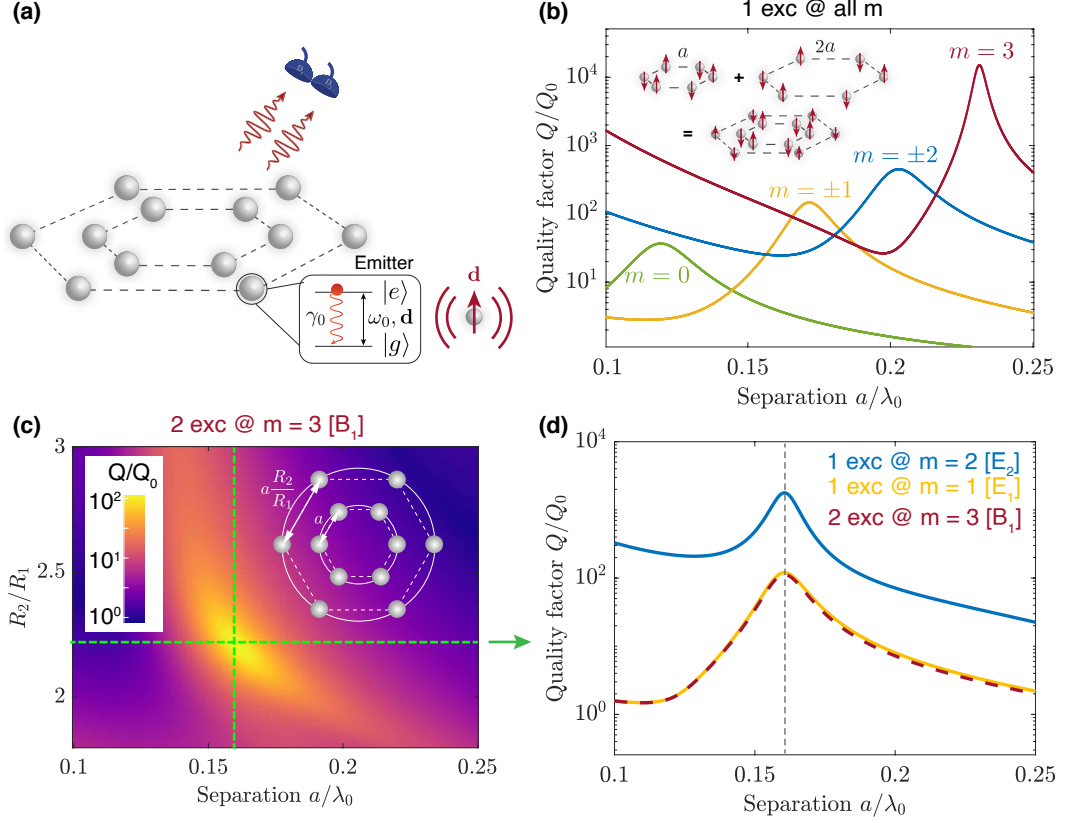


Figure 1 – (a) Scheme of the considered structure (oligomer) of quantum emitters arranged in two concentric rings supporting the eigenstates with angular quasi-momentum m . For rings of six emitters, $m \in \{0, \pm 1, \pm 2, 3\}$. The oligomer is placed in xy -plane. The quantum emitter is a two-level system with resonant frequency ω_0 , spontaneous emission rate γ_0 , and transition electric dipole moment $\mathbf{d} \parallel z$. (b) Quality factors (Q-factors) of *high-Q* singly excited eigenstates of the oligomer Q_m for all m . Q is normalized by $Q_0 = \omega_0/\gamma_0$ and plotted as a function of separation between emitters a/λ_0 where $\lambda_0 = 2\pi c/\omega_0$. The high-Q state with m is the result of the alignment of ring states with the same m into an anti-symmetric combination, as shown in the inset for $m = 3$. (c) Dependence on the ring parameters (shown in inset) of Q-factor for doubly excited state with $m = 3$ such that $Q^{-1} = Q_1^{-1} + Q_2^{-1}$ where Q_1^{-1} and Q_2^{-1} are Q-factors of singly excited states from subfigure (b) with $m = 1$ and $m = 2$. (d) Q-factor of this doubly excited state (burgundy dashed curve) and Q-factor of singly excited states with $m = 1$ (yellow) and $m = 2$ (blue) vs a for $R_2/R_1 = 2.2$

In the **second chapter**, we present singly excited eigenstates of a single ring of N emitters polarized in a transverse direction and introduce angular quasi-

momentum m of the state. We formulate effective equations for finding singly and doubly excited eigenstates and their spectra in single- and multi-ring structures. We also derive the number of singly and doubly excited states with angular quasi-momentum m for single- and multi-ring structures. In particular, it is shown that one excitation in a single ring can be described by a single amplitude and two excitations can be described by $\sim N/2$ amplitudes for a given m . In this chapter, we also perform a symmetry classification of the eigenstates for a ring of $N = 6$ emitters using group theory, essentially, we derive the correspondence between m and the irreducible representation of the symmetry group of a ring C_{6v} . The symmetry classification is used further to obtain selection rules for terms in the expansion of a doubly excited state over the products of singly excited states. A necessary and sufficient condition is the presence of an irreducible representation of a doubly excited state in the product of irreducible representations of singly excited states. It follows from this that the angular quasi-momentum of a doubly excited state is the sum of the angular quasi-momentum of singly excited states.

In the **third chapter**, we study the subradiant properties of eigenstates in ring oligomers. We introduced a mechanism based on the interaction of two subsystems of emitters supporting the states with the same symmetry in order to obtain high-Q states. Then we consider an oligomer, composed of a ring and a central emitter, that supports a high-Q state with only angular quasi-momentum $m = 0$. In order to obtain high-Q states with $m \neq 0$, we replace a central emitter with a second ring of a smaller radius and the same number of emitters shown in figure 1(a). Both rings support the states with all values of m that can interact and form anti-symmetric superposition with suppressed radiative losses as shown in figure 1(b). Moreover, we show that two rings of six emitters support a doubly excited state with $m = 3$ such that its Q-factor is a sum of the Q-factor of high-Q singly excited states with $m = 1$ and $m = 2$ (or $m = -1$ and $m = -2$): $Q^{-1} = Q_1^{-1} + Q_2^{-1}$. By varying the ring radii R_2/R_1 and separation between emitters a/λ_0 as shown in figure 1(c), we find the optimal parameters maximizing the Q-factor of the doubly excited state. For the optimal parameters, Q-factors of singly excited states Q_1 and Q_2 have maxima, therefore the Q-factor of the doubly excited state also has a maximum where $Q/Q_0 \approx 110$ [see figure 1(d)]. We also show that this doubly excited state enters B_1 irreducible representation which is contained only in the product of irreducible representations E_1 and E_2 of singly excited states with $m_1 = 1$ and

$m_2 = 2$, although the total angular quasi-momentum of singly excited states with $m_0 = 1$ and $m_3 = 2$ is also equal three. The radiative properties of these states are also studied.

1 THEORETICAL DESCRIPTION OF QUANTUM EMITTER ENSEMBLES

1.1 Effective Hamiltonian and spontaneous emission of radiation

Consider a free-space ensemble of N identical quantum emitters of the hydrogen-like type so that each emitter consists only of nuclei and a single electron. Assume that the emitters are perfectly trapped around their positions at zero temperature, therefore one can introduce perfectly defined coordinates of emitters \mathbf{r}_i without any thermal fluctuations. Let us also suppose that the electron in the emitter can occupy only two levels, namely ground $|g_i\rangle$ and excited $|e_i\rangle$ ones, with an allowed optical transition between them at the resonant frequency ω_0 [see figure 2(a)]. Here the subscript i is introduced only to distinguish emitters. To describe the absorption and the emission of excitation by an atom, one can define the ladder operators, $\hat{\sigma}_i^\dagger = |e_i\rangle \langle g_i|$ the creation operator and $\hat{\sigma}_i = |g_i\rangle \langle e_i|$ the annihilation operator for the i -th emitter [see figure 2(b)]. In this regard, the Hamiltonian of “free” emitters can be written as $\hat{H}_{\text{emitters}} = \sum_{i=1}^N \hbar\omega_0 \hat{\sigma}_i^\dagger \hat{\sigma}_i$ where \hbar is the Planck constant.

From a theoretical point of view, the two-level approximation for emitters is attractive because, first, it describes well real optical emitters such as atoms, ions, quantum dots, dye molecules, and superconducting qubits. Secondly, the interaction of a two-level system with a quantized electromagnetic field in free space is extensively covered in the literature [6, 38, 39]. Let us present the key points of this formalism.

Since the size of a quantum emitter is much smaller than the optical wavelength, the interaction of the emitter with an electromagnetic field can be described in the dipole approximation. For a two-level system, the operator of the electric dipole moment is $\hat{\mathbf{d}}_i = \mathbf{d}\sigma_i + \mathbf{d}^*\sigma_i^\dagger$ where $\mathbf{d} = \langle g_i | \hat{\mathbf{d}}_i | e_i \rangle$ is so-called transition dipole moment that is identical for all emitters. In the dipole approximation, the exchange of excitations between emitters and electromagnetic modes can be cast by Tavis-Cummings Hamiltonian $\hat{H}_{\text{int}} = \sum_{i=1}^N \hat{\mathbf{d}}_i \cdot \hat{\mathbf{E}}(\mathbf{r}_i)$ where $\hat{\mathbf{E}}(\mathbf{r}_i)$ is the electric field operator composed of an infinite set of plane waves in free space [40].

In order to eliminate electromagnetic degrees of freedom, we implement a standard procedure based on their integration in the Born-Markov approximation [41, 42]. Note that the Born-Markov approximation is applicable because

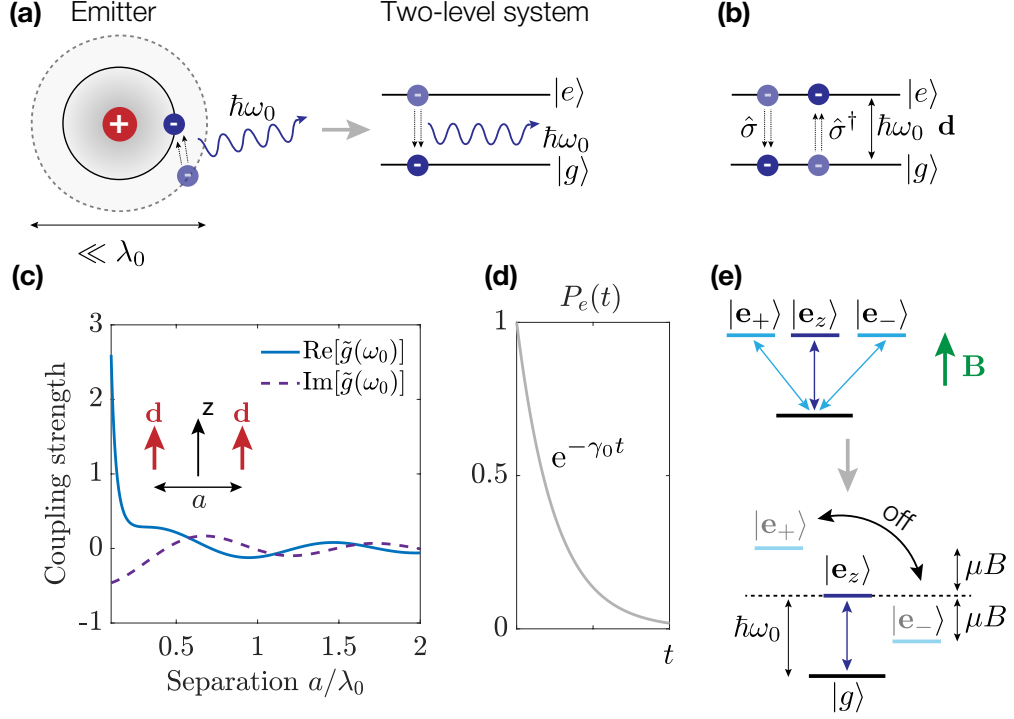


Figure 2 – (a) Two-level approximation for a quantum emitter. (b) The ladder operators (σ^\dagger and σ), resonant frequency (ω_0), and dipole moment (\mathbf{d}) of the transition in the two-level system from ground state $|g\rangle$ to excited one $|e\rangle$. (c) Real and imaginary parts of quasi-resonant coupling strength (4) in units of $\hbar\gamma_0$. The coupling strength $\tilde{g}(\omega_0)$ is plotted for two emitters polarized perpendicular to the connection axis and separated by a/λ_0 where $\lambda_0 = 2\pi c/\omega_0$ (see inset). (d) The population of the excited state for a single emitter as a function of time. γ_0 is the inverse lifetime (natural linewidth) of a single emitter. (e) Zeeman splitting of excited level due to an external magnetic field $\mathbf{B} \parallel \mathbf{e}_z$

the relaxation time of the reservoir (radiation continuum in the vacuum) is zero at zero temperature [43] and is smaller than the relaxation time of the emitter system. We will not go here through this formalism in detail, however, we will give an intuitive explanation of the result written below. By an analogy with a classical coupled-electric-dipole equation [44, 45], it is natural to suppose that an emitter $\hat{\sigma}_i$ is driven by a quantized field at position \mathbf{r}_i which is rescattered by other emitters and depends only their positions via electromagnetic Green's tensor $\hat{\mathbf{G}}(\mathbf{r}_i, \mathbf{r}_j, \omega)$ [see section 1.4]. Indeed, both the classical and quantized fields should satisfy the same wave equation [see equation (12) below]. Moreover, the emitters are actually atoms with a very narrow linewidth of the response, hence, the dependence of Green's tensor can be approximated as $\hat{\mathbf{G}}(\mathbf{r}_i, \mathbf{r}_j, \omega) \approx \hat{\mathbf{G}}(\mathbf{r}_i, \mathbf{r}_j, \omega_0)$ –quasi-resonant or Markov approximation.

Thus, a quantized electromagnetic field can be written via the replacement of classical dipole moments by their quantum counterparts $\mathbf{d}_i \rightarrow \hat{\mathbf{d}}_i$ which in the absence of an external field reads [42]:

$$\hat{\mathbf{E}}^\dagger(\mathbf{r}, \omega_0) = \frac{\omega_0^2}{\epsilon_0 c^2} \sum_{i=1}^N \hat{\mathbf{G}}(\mathbf{r}, \mathbf{r}_i, \omega_0) \cdot \mathbf{d} \hat{\sigma}_i, \quad (1)$$

where c is the speed of light in vacuum, ϵ_0 is the vacuum dielectric permittivity. The superscript \dagger indicates positive frequency components $\omega > 0$.

If we formally substitute (1) into the light-matter interaction Hamiltonian $\hat{H}_{\text{int}} = \sum_{i=1}^N \hat{\mathbf{d}}_i \cdot \hat{\mathbf{E}}(\mathbf{r}_i)$, we can expect to obtain the following effective, non-Hermitian Hamiltonian $\hat{H}_{\text{eff}} = \hat{H}_{\text{emitters}} + \hat{H}_{\text{int}} = \sum_{i=1}^N \hbar \omega_0 \hat{\sigma}_i^\dagger \hat{\sigma}_i + \sum_{i,j=1}^N g_{ij}(\omega_0) \hat{\sigma}_i^\dagger \hat{\sigma}_j$, where the coupling strength between emitters $g_{ij}(\omega_0) = -\frac{\omega_0^2}{c^2 \epsilon_0} \mathbf{d}^\dagger \cdot \hat{\mathbf{G}}(\mathbf{r}_i, \mathbf{r}_j, \omega_0) \cdot \mathbf{d}$.

Further, one will consider only the emitters with the orientation of \mathbf{d} along z axis, perpendicular to xy plane containing the emitters. In this case, the coupling strength turns to $g_{ij}(\omega_0) = -\frac{\omega_0^2 |\mathbf{d}|^2}{c^2 \epsilon_0} G_{zz}(|\mathbf{r}_i - \mathbf{r}_j|, \omega_0)$ with G_{zz} the element of free-space Green's tensor (16) depending only on the relative distance between emitters $|\mathbf{r}_i - \mathbf{r}_j|$ for the transverse polarization of \mathbf{d} . Note that the real part of g_{ij} is the strength of coherent coupling between dipoles via the exchange of photons whereas the imaginary part of g_{ij} is the rate of dissipative coupling. Figure 2(c) shows the real and imaginary parts of g_{ij} for a case of two transverse emitters separated by the length a . One can see the oscillatory behavior of coupling strength with the increase of a , therefore, the radiative properties of emitter ensembles strongly depend on the ensemble geometry.

It is important to take the limit of g_{ij} for $a/\lambda_0 \rightarrow 0$ corresponding to g_{ii} . One can see in figure 2(c) that $\text{Re}[g_{ij}]$ is divergent at $a/\lambda_0 \rightarrow 0$, however, it is just a limitation of the dipole-dipole coupling model for small separations. This issue can be overcome by the Green's function renormalization yielding a finite $\text{Re}[g_{ii}]$ called the Lamb shift [46]. The Lamb shift is typically much smaller than ω_0 [47], and we assume that it is already incorporated in the definition of ω_0 . It is more interesting to take a look at $\text{Im}[g_{ii}]$ which remains finite. One can obtain it

as $\text{Im}[g_{ii}] = -\frac{\hbar\gamma_0}{2}$ where

$$\gamma_0 = \frac{\omega_0^3 |\mathbf{d}|^2}{3\pi\hbar c^3 \epsilon_0}. \quad (2)$$

We note that γ_0 has a meaning of the doubled imaginary part of complex energy (its natural linewidth) for a single emitter $\hbar\left(\omega_0 - i\frac{\gamma_0}{2}\right)$. One can write the evolution of the probability amplitude for the emitter in the excited state at $t = 0$ as $c_e(t) = e^{-i(\omega_0 - i\frac{\gamma_0}{2})t}$. Hence, γ_0 is also the decay rate of the excited state population $P_e(t) = |c_e(t)|^2 = e^{-\gamma_0 t}$ due to the losses of energy via the radiation into free-space electromagnetic modes [see figure 2(d)]. In literature, such a regime of light-matter interaction is called a weak coupling [6]. In the presented model, a weak coupling manifests itself in the magnitude of coupling strength (4). One can see in figure 2(c) that $|\text{Re}[g_{ij}|], |\text{Im}[g_{ij}|] \sim \hbar\gamma_0 \ll \hbar\omega_0$ for atomic emitters ($\gamma_0/2\pi \sim 10$ MHz, $\omega_0/2\pi \sim 300$ THz [25]). It also justifies the use of quasi-resonant approximation for the coupling strength.

To sum up, one can consider a quantum emitter as a two-level system with the resonant frequency ω_0 , the dissipation rate γ_0 , and interacting with the electromagnetic field as an electric dipole \mathbf{d} . Let us discuss the possibility of obtaining two distinct isolated levels in a realistic atom. It should be noted that atoms exhibit numerous energy levels characterized by fine and hyperfine structures. For the sake of simplicity, let us consider an atom with a single electron residing in a nuclear potential that possesses spherical symmetry. This model represents the simplest yet realistic depiction of hydrogen-like atoms. Within this model, there is allowed electric dipole transition from the ground level (1s) to the excited level (2p). However, this transition exhibits a three-fold degeneracy with respect to the polarization of the transition dipole moment, namely out-of-plane \mathbf{e}_z and two in-plane $\mathbf{e}_\pm = \mp(\mathbf{e}_x \pm i\mathbf{e}_y)$ ones, which can be excited by a linearly or circularly polarized light [see figure 2(e)]. The degeneracy can be eliminated by an external, strong magnetic field \mathbf{B} which induces the Zeeman splitting of the atomic levels such that $|\mu B| \gg \gamma_0$ where μ is the magnetic moment of an atom [see figure 2(e)].

In a weak coupling regime, the ensemble of N identical dipole emitters can be described by the following effective Hamiltonian:

$$\hat{H}_{\text{eff}} = \sum_{i=1}^N \hbar \left(\omega_0 - i \frac{\gamma_0}{2} \right) \hat{\sigma}_i^\dagger \hat{\sigma}_i + \sum_{i=1}^N \sum_{\substack{j=1, \\ j \neq i}}^N \tilde{g}_{ij}(\omega_0) \hat{\sigma}_i^\dagger \hat{\sigma}_j, \quad (3)$$

where a quasi-resonant, normalized coupling strength for transverse emitters $\mathbf{d} \parallel \mathbf{e}_z$ is given by:

$$\tilde{g}_{ij}(\omega_0) = \frac{g_{ij}(\omega_0)}{\hbar \gamma_0} = -\frac{3\pi c}{\omega_0} G_{zz}(|\mathbf{r}_i - \mathbf{r}_j|, \omega_0). \quad (4)$$

1.2 Effective Schrödinger equation

Following the emergence of the basics of the theory concerning the interaction between two-level systems and the electromagnetic reservoir (vacuum) modes, it becomes possible to explore the characteristics exhibited by the eigenstates of collections of two-level systems. The eigenstates along with the corresponding eigenenergies of effective Hamiltonian (3) can be found from effective Schrödinger equation:

$$\hat{H}_{\text{eff}} |\psi\rangle = \varepsilon |\psi\rangle, \quad (5)$$

where $|\psi\rangle$ is the collective eigenstate of the system, and ε is the complex eigenenergy that can be written in $\varepsilon = \hbar \left(\omega - i \frac{\gamma}{2} \right)$ form. Here the real part ω is the angular frequency of the eigenstate while the imaginary part $\gamma/2$ defines the collective decay rate of the state.

We need to make also an important remark about the eigenstates $|\psi\rangle$ of (5). For a single emitter, the excited state $|e\rangle$ with energy $\hbar \left(\omega_0 - i \frac{\gamma_0}{2} \right)$ is a solution of equation (5). Let us assume that the emitter occupies this state at $t = 0$. Since the probability $P_e(t)$ decays with time [see figure 2(d)], then, strictly speaking, the ket-vector $|e\rangle$ can be associated with the emitter only at $t = 0$. To study the rigorous dynamics of the system for $t > 0$, it is necessary to solve the Lindblad equation for the density matrix of the emitter subsystem. Nevertheless, we can call the state $|e\rangle$ as the eigenstate of the system at $t = 0$. Hence, since our primary

interest is the spectrum of an ensemble but not its time evolution, we can will solve equation (5) instead of the Lindblad equation.

To conclude this subsection, let us mention that, for numerical diagonalization of \hat{H}_{eff} , it is convenient to do the following transformation of (3): $\hat{H}_{\text{eff}} \rightarrow \tilde{\hat{H}}_{\text{eff}} = \frac{1}{\hbar\gamma_0} \left(\hat{H}_{\text{eff}} - \hbar\omega_0 \hat{I} \right)$. In this regard, Schrödinger equation (5) should be rewritten as

$$\begin{aligned} \tilde{\hat{H}}_{\text{eff}} |\psi\rangle &= \underbrace{\frac{\varepsilon - \hbar\omega_0}{\hbar\gamma_0}}_{\tilde{\varepsilon}} |\psi\rangle, \\ \tilde{\hat{H}}_{\text{eff}} &= \sum_{i=1}^N \hbar \left(-\frac{i}{2} \right) \hat{\sigma}_i^\dagger \hat{\sigma}_i + \sum_{i=1}^N \sum_{\substack{j=1, \\ j \neq i}}^N \tilde{g}_{ij}(\omega_0) \hat{\sigma}_i^\dagger \hat{\sigma}_j, \end{aligned} \quad (6)$$

where $\tilde{\varepsilon}$ the shifted and normalized eigenenergy is introduced. After applying this transformation the calculated spectrum does not depend on particular numerical values of ω_0 , and γ_0 .

1.3 Singly and doubly excited collective states

We can note that effective Hamiltonian (3) preserves the total number of excitations in the system. Thus, the whole infinite-dimensional Hilbert space \mathcal{H} of states of the system can be decomposed into a series of subspaces (manifolds) as follows

$$\mathcal{H} = \mathcal{H}_0 + \mathcal{H}_1 + \mathcal{H}_2 + \mathcal{H}_3 + \dots + \mathcal{H}_N, \quad (7)$$

where \mathcal{H}_n is the subspace corresponding to the case of n excitations in the system, N is the total number of emitters. For the last term in the expansion, $n = N$ because N two-level emitters cannot contain more than N excitations. The proper analogy for this expansion is the space of quantum oscillator eigenstates: The eigenstates are characterized by the number n .

To understand the physical meaning of expansion terms \mathcal{H}_n , let us consider several cases of different n numbers of excitations.

- a) $n = 0$: There are no excitations in the system, therefore all the N emitters occupy the ground state. Thus, \mathcal{H}_0 the subspace consists only of one state

$|G\rangle = |g\rangle^{\otimes N} \equiv \underbrace{|g\rangle \otimes |g\rangle \otimes \dots \otimes |g\rangle}_{N \text{ times}}$ with a zero energy usually referred to in the literature as a ground state of the ensemble;

b) $n = 1$: There is a single excitation in the system. In this case, \mathcal{H}_1 the subspace consists of N states that can be written in the following way

$$|\psi\rangle = \sum_{i=1}^N c_i |e_i\rangle, \quad (8)$$

with $|e_i\rangle = \hat{\sigma}_i^\dagger |g\rangle^{\otimes N}$ being the basis state with only i -th atomic emitter excited, while the rest are in the ground state [see figure 3]. Let us plug (8) into Schrödinger equation (6). This ansatz yields a set of N linear algebraic equations on single-excitation probability amplitudes c_i of excitation on i -th emitter:

$$\tilde{\varepsilon} c_i = -\frac{i}{2} c_i + \sum_{\substack{j=1, \\ j \neq i}}^N \tilde{g}_{ij}(\omega_0) c_j, \quad (9)$$

with the eigenenergy $\tilde{\varepsilon}$ defined by (6), and $\tilde{g}_{ij}(\omega_0)$ given by (4).

c) $n = 2$: The doubly excited state is

$$|\Psi\rangle = \sum_{i=1}^N \sum_{j=i+1}^N c_{ij} |e_i e_j\rangle, \quad (10)$$

where $|e_i e_j\rangle = \hat{\sigma}_i^\dagger \hat{\sigma}_j^\dagger |g\rangle^{\otimes N}$ is the state with excited both i - and j -th atomic emitters [see figure 3]. The limits in sums are taken because of two following facts. The considered emitters have only two energy levels, therefore two excitations cannot be located at the same emitter, then $i \neq j$. The emitters and excitations are identical, hence double-excitation probability amplitude is symmetric $c_{ij} = c_{ji}$. Combining these two properties of c_{ij} , one can consider only the amplitudes with $i > j$. Thus, for a system of N dipole emitters, the total amount of doubly excited eigenstates is $\frac{N(N-1)}{2}$ which can be obtained by solving the following system of $\frac{N(N-1)}{2}$ linear

equations:

$$\tilde{\epsilon}c_{ij} = -ic_{ij} + \sum_{k>i} \tilde{g}_{kj}(\omega_0)c_{ik} + \sum_{k<j} \tilde{g}_{ik}(\omega_0)c_{kj}. \quad (11)$$

Note that here and further capital Ψ is used to distinguish doubly excited kets from singly excited ones.

- d) $n > 2$: The dimension of \mathcal{H}_n equals to the binomial coefficient $C_N^n \equiv \frac{N!}{n!(N-n)!}$. It is easy to verify using this formula that $\dim \mathcal{H}_0 = 1$, $\dim \mathcal{H}_1 = N$, and $\dim \mathcal{H}_2 = \frac{N(N-1)}{2}$.

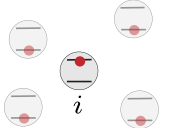
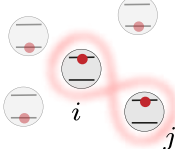
State	Basis	Wave function
Singly excited	 $ e_i\rangle$	$ \psi\rangle = \sum_{i=1}^N c_i e_i\rangle$
Doubly excited	 $ e_i e_j\rangle$	$ \Psi\rangle = \sum_{i=1}^N \sum_{j=i+1}^N c_{ij} e_i e_j\rangle$

Figure 3 – Summary on a basis and wave functions for singly excited and doubly excited eigenstates of the Hamiltonian (3)

Thus, the collective states of ensembles of quantum emitters can be classified, first of all, by the number of involved atomic (matter) excitations. As one can see, a growth of the excitation number significantly increases the dimensionality of the eigenvalue problem. This thesis focuses only on the cases of $n = 1$ and $n = 2$ excitations in order to limit the numerical effort. For singly and doubly excited eigenstates, we can calculate the eigenstates and eigenenergies as right-column eigenvectors and eigenvalues of equations (9) and (11), respectively.

1.4 Green's tensor in free space

The coupling strength between emitters (4) as well as the collective effects in their ensembles are governed by Green's tensor of the wave equation for the electromagnetic field.

In the frequency domain, the electromagnetic wave equation is written as [44]

$$\nabla \times \nabla \times \mathbf{E}(\mathbf{r}, \omega) - \epsilon(\mathbf{r}, \omega) \frac{\omega^2}{c^2} \mathbf{E}(\mathbf{r}, \omega) = \frac{\omega^2}{\epsilon_0 c^2} \mathbf{P}(\mathbf{r}, \omega), \quad (12)$$

where ∇ is the nabla operator, $\epsilon(\mathbf{r}, \omega)$ is the dielectric permittivity depending on the coordinate \mathbf{r} and frequency ω , and $\mathbf{E}(\mathbf{r}, \omega)$ is the classical electric field.

For a point dipole source located at \mathbf{r}' point, the polarization vector is $\mathbf{P}(\mathbf{r}, t) = \mathbf{d} \delta(\mathbf{r} - \mathbf{r}') e^{-i\omega t}$ with \mathbf{d} the electric dipole moment and $\delta(\mathbf{r} - \mathbf{r}')$ three-dimensional Dirac delta function. After replacing the right-hand side of (12) with the polarization in the dipole approximation $\mathbf{P}(\mathbf{r}, \omega) = \mathbf{d} \delta(\mathbf{r} - \mathbf{r}')$, equation (12) transforms to the following one:

$$\nabla \times \nabla \times \mathbf{E}(\mathbf{r}, \omega) - \epsilon(\mathbf{r}, \omega) \frac{\omega^2}{c^2} \mathbf{E}(\mathbf{r}, \omega) = \frac{\omega^2}{\epsilon_0 c^2} \mathbf{d} \delta(\mathbf{r} - \mathbf{r}'). \quad (13)$$

A particular solution of this equation (so-called scattered field) can be formally written as

$$\mathbf{E}(\mathbf{r}, \omega) = \frac{\omega^2}{\epsilon_0 c^2} \hat{\mathbf{G}}(\mathbf{r}, \mathbf{r}', \omega) \cdot \mathbf{d}, \quad (14)$$

which is electric field generated by an electric dipole.

Green's tensor obeys the following equation:

$$\nabla \times \nabla \times \hat{\mathbf{G}}(\mathbf{r}, \mathbf{r}', \omega) - \epsilon(\mathbf{r}, \omega) \frac{\omega^2}{c^2} \hat{\mathbf{G}}(\mathbf{r}, \mathbf{r}', \omega) = \delta(\mathbf{r} - \mathbf{r}') \hat{I}, \quad (15)$$

where \hat{I} is 3×3 identity matrix. Note that, in the above equation, the nabla operator ∇ differentiates with respect to the \mathbf{r} variable. For the case of free space, one should set $\epsilon(\mathbf{r}, \omega) = 1$ in equation (15). In this case, the solution is $\hat{\mathbf{G}}(\mathbf{r}, \mathbf{r}', \omega) = \hat{\mathbf{G}}_0(\mathbf{R}, \omega)$ with $\mathbf{R} = \mathbf{r} - \mathbf{r}'$ where

$$\hat{\mathbf{G}}_0(\mathbf{R}, \omega) = \frac{e^{ikR}}{4\pi R} \left\{ \left(1 + \frac{i1}{kR} - \frac{1}{k^2 R^2} \right) \hat{I} + \left(-1 - \frac{i3}{kR} + \frac{3}{k^2 R^2} \right) \frac{\mathbf{R} \otimes \mathbf{R}}{R^2} \right\} \quad (16)$$

with $R = |\mathbf{R}|$, $k = \omega/c$ the wavenumber, $\mathbf{R} \otimes \mathbf{R}$ the dyadic (tensor) product of radius-vector \mathbf{R} with itself [44].

In the presence of nanostructure or other non-homogeneous environments, Green's function involves not only a free space part but also a scattered component $\hat{\mathbf{G}} = \hat{\mathbf{G}}_0 + \hat{\mathbf{G}}_{\text{sca}}$ that can modify both the resonant frequency ω_0 and the emission rate γ_0 of a single emitter.

In this chapter, we introduced effective Schrödinger equation with non-Hermitian Hamiltonian describing the coupling between dipole emitters in free space and eigenstates in Born-Markov approximation. In particular, one- and two-excitation manifolds were considered.

2 EIGENSTATES OF A SINGLE RING AND MULTIRING ENSEMBLES OF EMITTERS

Chapters 2 and 3 are devoted to the modeling of eigenstates of single- and multi-ring structures as well as to the investigation of their subradiant properties.

2.1 The single excitation spectrum of a ring. Angular quasi-momentum

Using the formalism from Chapter 1, let us first find singly excited eigenstates of a single ring of N_p emitters located in free space. The ring is shown schematically in Figure 4. Let us also assume that all emitters have the transversely oriented transition dipole moments $\mathbf{d} \parallel \mathbf{e}_z$. The ring is located in xy -plane such as its center coincides with the origin of the Cartesian coordinate system. The emitters are placed at the vertices of a regular polygon with N_p edges. In this case, the radius vector of the position for i -th emitter in a ring is

$$\mathbf{r}_i = R (\cos \varphi_i, \sin \varphi_i, 0)^T, \quad i = 1..N_p, \quad (17)$$

where R is the ring radius, and $\varphi_i = (i - 1)2\pi/N_p$ is the angular coordinate of i -th emitter. Thus, the distance between neighboring emitters in the ring is the same for all emitters and equals $a = 2R \sin(\pi/N_p)$. Since the spectrum and eigenstates are the subjects of our interests, there are no external electromagnetic or other fields.

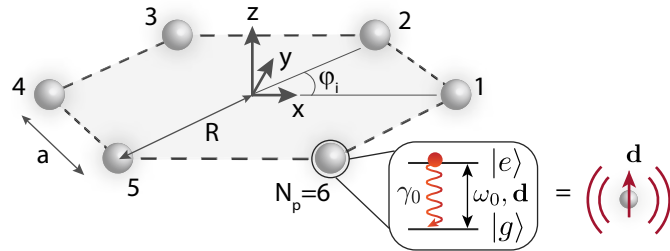


Figure 4 – Scheme of a single ring of N_p two-level dipole emitters placed in xy -plane ($N_p = 6$ here). The emitters with subwavelength separation distance a are arranged in a regular equilateral polygon along a circle of radius R . The angular coordinate of i -th emitters is shown as $\varphi_i = 2\pi(i - 1)/N_p$. The parameters of two-level emitters are the same as in figure 1

To calculate the single excitation spectrum of a ring of emitters shown in figure 4, we use equation (9). Since a ring of dipoles preserves rotational symmetry along z -axis ($C_{N_p, v}$ point symmetry group), the eigenstates of a ring can be described by the angular quasi-momentum m [29, 33]. The meaning of m is

the following: for the state of a ring with the angular quasi-momentum m , the phase shift between the amplitudes of neighboring emitters c_{i+1} and c_i equals $\Delta\varphi(m) = 2\pi m/N_p$. The prefix “quasi” in the name of the m indicates that it is determined up to the number of emitters in a ring N_p because the values of angular quasi-momentum m and $(m + nN_p)$, where n is an integer, correspond to the same phase shifts $\Delta\varphi(m + nN_p) = \Delta\varphi(m) + 2\pi n$, hence the identical physical states of the system. The direct analogy for the angular quasi-momentum for the systems with rotational symmetry is the quasi-wavevector or Bloch wavevector for the systems with translational symmetry which is defined up to the reciprocal lattice vector. Furthermore, one can introduce “the first Brillouin zone” of values for the m as a set $\{0, \pm 1, \pm 2, \dots, \pm (N_p - 2)/2, N_p/2\}$ for even N_p , or $\{0, \pm 1, \pm 2, \dots, \pm (N_p - 2)/2, \pm (N_p - 1)/2\}$ for odd N_p .

The number of states for different parities of m is summarized in figure 5. Note that, for even N_p , the maximum angular quasi-momentum with opposite sign $m = -N_p/2$ corresponds to the same phase shift of $\Delta\varphi(m = \pm N_p/2) = \pi$ between neighboring emitters and, consequently, the same state. For convenience, we choose a positive sign $m = N_p/2$.

Number of values of m	N_p is even		N_p is odd	
	$\frac{N_p}{2}$ is even	$\frac{N_p}{2}$ is odd	$\frac{(N_p + 1)}{2}$ is even	$\frac{(N_p + 1)}{2}$ is odd
even m	$\frac{N_p}{2}$	$\frac{N_p}{2}$	$\frac{(N_p - 1)}{2}$	$\frac{(N_p + 1)}{2}$
odd m	$\frac{N_p}{2}$	$\frac{N_p}{2}$	$\frac{(N_p + 1)}{2}$	$\frac{(N_p - 1)}{2}$

Figure 5 – Number of eigenstates with even or odd angular quasi-momentum m (rows) for different parities of N_p number of emitters in a ring (columns). Note that the sum of the values in each column equals the total number of singly excited eigenstates N_p

Thus, the spectrum of a ring can be calculated using the following ansatz for the excitation amplitudes c_i :

$$c_i = c^{(m)} e^{im\varphi_i}, \quad (18)$$

where $c^{(m)}$ is the analog of periodic Bloch amplitude for a ring. After inserting (18) in equation (9), one obtains a set of energies of N_p singly excited eigenstates for a ring:

$$\tilde{\varepsilon}_{\text{ring}}^{(m)} = -\frac{i}{2} - \frac{3\pi c}{\omega_0} \sum_{i=2}^{N_p} G_{zz}(|\mathbf{r}_1 - \mathbf{r}_i|, \omega_0) e^{im\varphi_i}, \quad (19)$$

or equivalently

$$\tilde{\varepsilon}_{\text{ring}}^{(m)} = -\frac{i}{2} - \frac{3}{4} \Sigma^{(m)}(R, N_p), \quad (20)$$

where $\Sigma^{(m)}(R, N_p)$ is the dipole sum for the state with the angular quasi-momentum m in a ring of radius R and of N_p emitters:

$$\Sigma^{(m)}(R, N_p) = \frac{4\pi c}{\omega_0} \sum_{i=2}^{N_p} G_{zz}(|\mathbf{r}_1 - \mathbf{r}_i|, \omega_0) e^{im\varphi_i}. \quad (21)$$

For a ring of $N_p = 6$ emitters and the separation between neighboring emitters a , the dipole sums are

$$\begin{aligned} \Sigma^{(m)}(R, N_p = 6) &= \frac{8\pi c}{\omega_0} \left[G_{zz}(a, \omega_0) \cos\left(\frac{\pi m}{3}\right) \right. \\ &\left. + G_{zz}(\sqrt{3}a, \omega_0) \cos\left(m\frac{2\pi}{3}\right) + \frac{1}{2} G_{zz}(2a, \omega_0) \cos(\pi m) \right]. \end{aligned} \quad (22)$$

One can notice that dipole sums (22) for $N_p = 6$ emitters are symmetric with respect to a sign of m that can be shown for any number of emitters N_p . Thus, the exchange of a quasi-momentum sign $m \leftrightarrow -m$ conserves energy $\tilde{\varepsilon}^{(m)} = \tilde{\varepsilon}^{(-m)}$. Hence, the ring eigenstates [see equation (26)] are doubly degenerate except for two cases. The state with $m = 0$ is non-degenerate for any N_p , and the state with $m = N_p/2$ has also no degeneracy for even N_p .

Equation (6) implies that a set of dimensional energies $\varepsilon^{(m)}$ can be obtained from a set of dimensionless eigenvalues $\tilde{\varepsilon}^{(m)}$ as follows

$$\varepsilon_{\text{ring}}^{(m)} = \hbar\omega_0 + \hbar\gamma_0 \times \tilde{\varepsilon}_{\text{ring}}^{(m)}. \quad (23)$$

On the other hand, $\varepsilon^{(m)} = \hbar \left(\omega_{\text{ring}}^{(m)} - i \frac{\gamma_{\text{ring}}^{(m)}}{2} \right)$, therefore one obtains the frequency of the collective ring state as

$$\omega_{\text{ring}}^{(m)} = \omega_0 - \frac{3\gamma_0}{4} \text{Re} \left[\Sigma^{(m)} (R, N_p) \right], \quad (24)$$

and its collective decay rate as

$$\gamma_{\text{ring}}^{(m)} = \gamma_0 + \frac{3\gamma_0}{2} \text{Im} \left[\Sigma^{(m)} (R, N_p) \right]. \quad (25)$$

Thus, the resonant frequency and emission rate of the emitter can be modified not only by the presence of a non-homogenous environment but also by the collective emitter-emitter interactions via the real and imaginary parts of the dipole sum, respectively.

Eigenenergies (20) correspond to the set of singly excited eigenstates $|\psi^{(m)}\rangle = \sum_{i=1}^{N_p} c_i |e_i\rangle$ with c_i the excitation probability amplitudes (18). In order to find $c^{(m)}$ in equation (18), let us remind the expression for the total probability to find an excitation on the ring. The total probability expression $\sum_{i=1}^{N_p} |c_i|^2 = 1$ implies that $c^{(m)} = \frac{1}{\sqrt{N_p}}$ for a single ring, therefore one can write the singly excited eigenstates as

$$|\psi_{\text{ring}}^{(m)}\rangle = \frac{1}{\sqrt{N_p}} \sum_{i=1}^{N_p} e^{im\varphi_i} |e_i\rangle. \quad (26)$$

Recall that $|e_i\rangle = \hat{\sigma}_i^\dagger |g\rangle^{\otimes N_p}$ is the state where the excitation is fully localized at i -th emitter.

2.2 Relation between angular quasi-momentum and irreducible representation

Let us look at how the ring states (26) are transformed under the rotation of a ring in xy -plane by $\varphi' = 2\pi/N_p$ angle around z axis in the clockwise direction. It is shown in figure 6(a) for a ring of $N_p = 6$ emitters when $\varphi' = \pi/3$. One can associate this operation with an operator of rotation $\hat{R}(\varphi')$. Note that such a rotation does the following permutation of indices of excitation amplitudes $i \rightarrow i' = (i+1)$

mod N_p [see figure 6(a)]. Hence, the matrix of $\hat{R}(\varphi')$ in the basis of singly excited states $\{|e_i\rangle\}_{i=1}^{N_p}$ has the following entries: $R_{ij}(\varphi') = \delta_{j,i'}$ for $\{i,j\} \in \{1..N_p\}$ where $\delta_{j,i'}$ is the Kronecker delta. From equation (18), it follows that $c_{i+1} = e^{im\varphi'} c_i$. Hence, one can write the action of $\hat{R}(\varphi')$ operator on eigenstates (26) as follows

$$\hat{R}(\varphi') \left| \psi^{(m)} \right\rangle = e^{im\varphi'} \left| \psi^{(m)} \right\rangle. \quad (27)$$

Thus, the rotation operator \hat{R} and effective Hamiltonian \hat{H}_{eff} are diagonalizable in the same basis (26) with the eigenvalue sets $\{e^{im\varphi'}\}$ and $\{\tilde{\varepsilon}^{(m)}\}$, respectively. This is reflected in a fact that the operators commute $\hat{H}_{\text{eff}}\hat{R} = \hat{R}\hat{H}_{\text{eff}}$.

Note that the operation of rotation of a ring by $\varphi' = 2\pi/N_p$ angle is included in transformations from the symmetry group of the ring of transverse emitters $C_{N_p,v}$. The structure is converted into itself after symmetry transformations consisting of rotations and reflections. For example, the symmetry group of a ring of six emitters C_{6v} consists of the rotation by $\pi/3$ angle around the z axis denoted in group theory as $C_6(z)$ [see figure 6(a)], the rotation $C_3(z)$ by $2\pi/3$ angle, the rotation $C_2(z)$ by π angle, and two reflections σ_v and σ_d relative to y and x axis, respectively, as shown in figure 6(b). All operators corresponding to these transformations can be diagonalized in the same basis $|\psi^{(m)}\rangle$ of eigenstates of \hat{H}_{eff} . Therefore, the Hamiltonian \hat{H}_{eff} commutes with all transformations of the symmetry group of the ring structures. Then the transformations from the symmetry group do not change the Hamiltonian (3) since they do not change the structure.

Here we can notice a deep connection of physics with group theory formulated by so-called Wigner's theorem. In simple words, this theorem can be formulated for Schrödinger equation (5) as follows. If the Hamiltonian remains invariant under transformations from the symmetry group, the eigenstates of such a Hamiltonian (3), which are solutions of the Schrödinger equation (5), are transformed by irreducible representations of the symmetry group. Thus, the symmetry of the eigenstate under transformations from the symmetry group is determined by the symmetry of the corresponding irreducible representation of the group.

Let us turn back to the example of a ring of six emitters with C_{6v} symmetry group. Figure 6(c) presents a character table for C_{6v} group with symmetry transformations and irreducible representations of the group. The irreducible representations are essentially the matrices acting on a column of functions

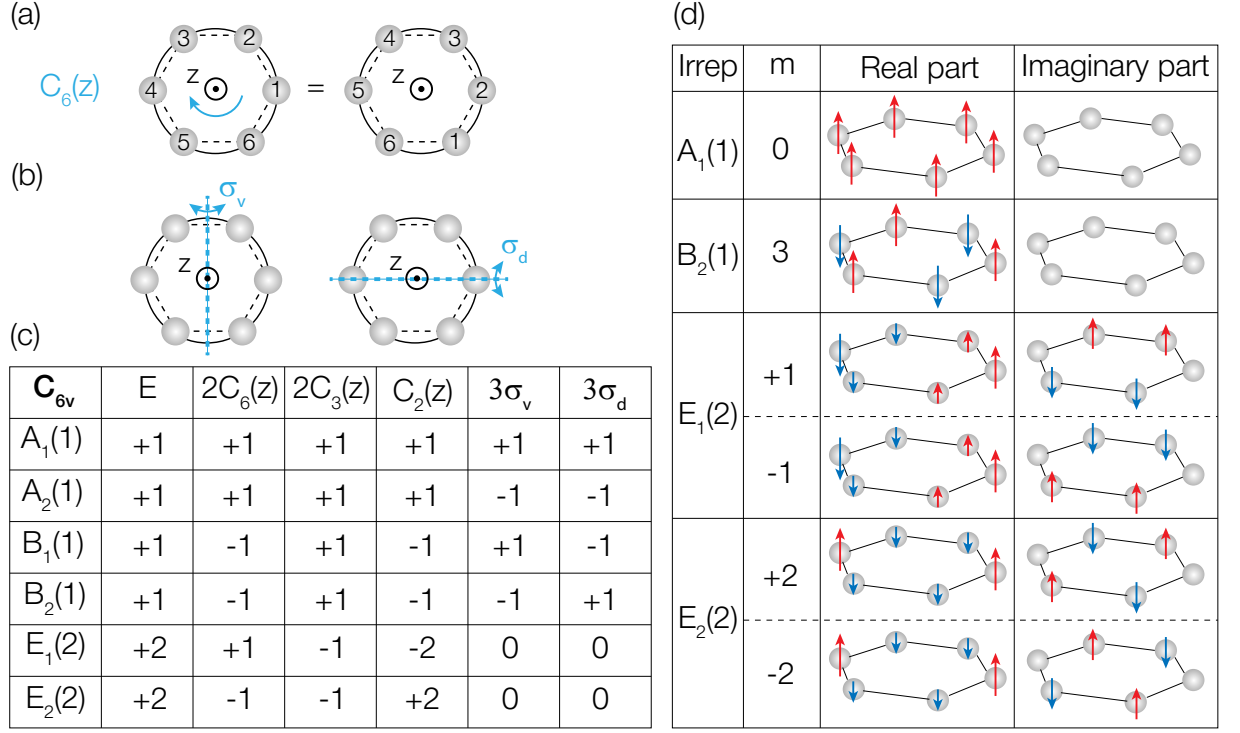


Figure 6 – (a) Altering of emitter indices after rotating the ring around z -axis by angle $2\pi/N_p$. (b) Reflection of the ring with respect to the axis passing between atoms (left) and through atoms (right). (c) Table of characters for C_{6v} symmetry group. The columns contain symmetry transformations, the rows correspond to irreducible representations with their dimensions in brackets. The cells show the trace (character) of irreducible representations for a given transformation. (d) Correspondence of the angular quasi-momentum m of singly excited states of a ring (26) for $N_p = 6$ to the irreducible representations (irreps) of the symmetry group of the ring (C_{6v}). The arrows show the real part $\propto \cos(m\varphi)$ and the imaginary part $\propto \sin(m\varphi)$ of the states. For clarity, the values with the same magnitude, but with different signs, are highlighted by different colors

$(\cos(m\varphi), \sin(m\varphi))^T$ under symmetry transformations, and the character is a trace of such a matrix. Let us identify the irreducible representations for the singly excited eigenstates (26) for a ring of six emitters. The excitation amplitudes of ring eigenstates (26) have real part $\propto \cos(m\varphi_i)$, and imaginary part $\propto \sin(m\varphi_i)$ where $\varphi_i = (i-1)\pi/3$ as shown in figure 6(d). It is obvious that the imaginary part is zero for $m = 0$ and $m = 3$, therefore these states should enter one-dimensional representations. For the states entering one-dimensional irreducible representations, we just need to multiply a state by a character in order to obtain a transformed state. The state with $m = 0$ has a homogenous distribution of amplitudes, therefore it remains the same under the symmetry transformations and enters trivial irreducible representation A_1 [see figure 6(c)]. The state with $m = 3$ is symmetric for the re-

flection σ_d [see figure 6(b)], therefore it enters B_2 representation [see figure 6(c)]. The modes with $m = \pm 1$ and $m = \pm 2$ have non-zero real and imaginary parts. Hence, they enter two-dimensional representations, E_1 or E_2 , and they are double degenerate [cf. equation (20)]. For these states, the real and imaginary parts have opposite symmetry with respect to the reflections, therefore they have zeros at corresponding cells in figure 6(c). Hence, let us take a look at the rotation by π around the z -axis $C_2(z)$. The irreducible representations E_1 and E_2 are 2×2 *diagonal* matrices for this rotation, therefore negative character (trace) “-2” corresponds to both anti-symmetric real and imaginary parts while the positive character “+2” is for both symmetric real and imaginary parts. The real and imaginary parts of states with $m = \pm 1$ (resp. $m = \pm 2$) are both anti-symmetric (resp. symmetric) with respect to this rotation, therefore the states with $m = \pm 1$ (resp. $m = \pm 2$) enter E_1 (resp. E_2) irreducible representation.

Thus, singly excited states of a ring of six emitters enter irreducible representations A_1 , B_2 , E_1 , and E_2 . Note that doubly excited states can enter other irreducible representations [see section 3.5].

2.3 Selection rules for expansions of doubly excited states

The symmetry analysis presented in section 2.2 can be helpful for the selection of non-zero coefficients in the expansion of doubly excited states over the products of singly excited states. For a doubly excited state $|\Psi^{(m)}\rangle$ with the defined angular quasi-momentum m , such an expansion can be written as follows

$$|\Psi^{(m)}\rangle = \sum_{m_1, m_2} v_{m_1, m_2} |\psi^{(m_1)}\rangle |\psi^{(m_2)}\rangle, \quad (28)$$

where $|\psi^{(m_1)}\rangle$ and $|\psi^{(m_2)}\rangle$ are singly excited states with angular quasi-momentum m_1 and m_2 , respectively. Expansion coefficients v_{m_1, m_2} can be considered as amplitudes of doubly excited state $|\Psi^{(m)}\rangle$ in reciprocal space of momentum as well as amplitudes c_{ij} describe this state in direct space of coordinates.

In the general case, a coefficient v_{m_1, m_2} is not equal to zero if the irreducible representation of doubly excited state $|\Psi^{(m)}\rangle$ is included in the expansion over the irreducible representations of the product of irreducible representations of $|\psi^{(m_1)}\rangle$ and $|\psi^{(m_2)}\rangle$ singly excited states.

Let us consider an example of C_{6v} symmetry group and write down expansions for all products of irreducible representations of singly excited eigenstates of

the ring [see figure 6(d)]:

$$\begin{aligned}
A_1 \times A_1 &= A_1, \\
A_1 \times B_2 &= B_2, \\
A_1 \times E_1 &= E_1, \\
A_1 \times E_2 &= E_2, \\
B_2 \times B_2 &= A_1, \\
B_2 \times E_1 &= E_2, \\
B_2 \times E_2 &= E_1, \\
E_1 \times E_1 &= A_1 + A_2 + E_2, \\
E_1 \times E_2 &= B_1 + B_2 + E_1, \\
E_2 \times E_2 &= A_1 + A_2 + E_1,
\end{aligned} \tag{29}$$

where \times is the product of representations. For instance, assume that a doubly excited state $|\Psi^{(m)}\rangle$ is transformed according to the irreducible representation B_2 . Thus, it can be composed of products of singly excited states entering A_1 and B_2 representations, or E_1 and E_2 representations. Otherwise, the coefficients $v_{m_1, m_2} \equiv 0$ for products of other singly excited states. Hence, $|\Psi^{(m)}\rangle$, transformed according to the representation B_2 , has angular quasi-moment $m = 3$ and can be obtained from pairs of the states with angular quasi-momentum $m_1 = 0$ (A_1) and $m_2 = 3$ (B_2), or $m_1 = 1$ (E_1) and $m_2 = 2$ (E_2), or $m_1 = -1$ (E_1) and $m_2 = -2$ (E_2). Thus, one can conclude that the sum of the angular quasi-momentum of singly excited states ($m_1 + m_2$) should be equal to the angular quasi-momentum of doubly excited state m . Hence, we obtain a weaker condition: The coefficient v_{m_1, m_2} can be zero or not if $m_1 + m_2 = m \pmod{N_p}$, but $v_{m_1, m_2} \equiv 0$ for $m_1 + m_2 \neq m \pmod{N_p}$.

In conclusion of this section, let us note that v_{m_1, m_2} coefficients in the most general case can be calculated as a solution of a system of linear equations $\mathbf{C}\mathbf{v} = \mathbf{v}_0$ where \mathbf{v} is a column vector of v_{m_1, m_2} coefficients of length N^2 , and \mathbf{v}_0 is a column vector of amplitudes c_{ij} of doubly excited state $|\Psi^{(m)}\rangle$ including $c_{ii} = 0$, and c_{ji} (recall that $c_{ji} = c_{ij}$). Entries of $N \times N$ matrix \mathbf{C} are defined as a product of amplitudes $c_i \times c_j$ from $|\psi^{(m_1)}\rangle$ and $|\psi^{(m_2)}\rangle$ singly excited states, respectively. The desired coefficients can be formally written as $\mathbf{v} = \mathbf{C}^{-1}\mathbf{v}_0$. Note that the

matrix \mathbf{C} always has a non-zero determinant because it is composed of products of amplitudes of orthogonal states.

2.4 Remark on the numerical calculation of degenerate eigenstates

The symmetry analysis is also helpful for the numerical calculation of the eigenstates of Hamiltonian (3). The eigenvalue problem can be solved, for example, in Matlab using the *eig* function. However, this method has a disadvantage regarding the calculation of degenerate eigenstates. Let $|\psi^{(m)}\rangle$ and $|\psi^{(-m)}\rangle$ be the “true” degenerate eigenstates with defined angular quasi-momentum m and $-m$. The numerical method, however, returns us their linear combinations $(a|\psi^{(m)}\rangle + b|\psi^{(-m)}\rangle)$ with a and b being the complex coefficients. These combinations are also the eigenstates of the Hamiltonian (3) but their angular quasi-momentum is not defined. How to overcome this difficulty?

One can employ transformations from the symmetry group of the structure. Choose a non-trivial transformation \hat{P} being a rotation or reflection from the symmetry group. Introduce a matrix V whose columns are the right eigenvectors for both operators \hat{H}_{eff} and \hat{P} . We also define diagonal matrices D_H and D_P as $D_H = V^{-1}\hat{H}_{\text{eff}}V$ and $D_P = V^{-1}\hat{P}V$ with the diagonal entries being eigenvalues of \hat{H}_{eff} and \hat{P} , respectively. If we calculate numerically the eigenvalues D_H and eigenvectors V directly from the diagonalization of \hat{H}_{eff} , we meet the problem mentioned above. However, we can first diagonalize the following operator $(\hat{H}_{\text{eff}} + r\hat{P})$ with r being a random real number. It can be noticed that this operator has the same eigenvectors V but a different spectrum $(D_H + rD_P)$. However, if we obtain the “true” eigenvectors V , we can calculate eigenenergies $D_H = V^{-1}\hat{H}_{\text{eff}}V$. Note that this method can be applied for rigorous numerical calculation of both singly and doubly excited states.

2.5 The single excitation spectrum of a multi-ring structure

Section 2.1 describes how to analytically calculate a single excitation spectrum and corresponding eigenstates of a ring with N_p emitters using the knowledge about the rotational symmetry of the structure. This helps to instantly obtain all N_p singly excited eigenstates energies with an angular quasi-momentum by calculating the dipole sums (21) for positive values of m instead of diagonalizing the $N_p \times N_p$ matrix.

This section considers structures of $N_r \neq 1$ concentric rings of N_p dipole emitters with $\{R_j\}_{j=1}^{N_r}$ radii placed in xy -plane. Thus, the total number of emit-

ters in the system is $N = N_r \times N_p$. An example of the geometry is illustrated schematically in figure 7.

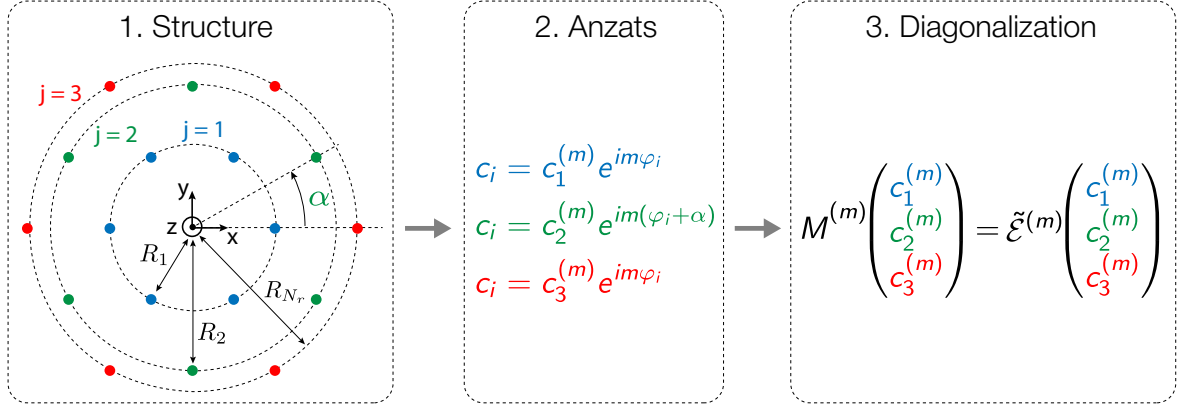


Figure 7 – A general approach to calculating the singly excited eigenstates with a defined angular quasi-momentum m for N_r concentric rings ($N_r = 3$ here). Each ring has N_p identical emitters ($N_p = 6$ here). First of all, we need to initialize the rings with their radii R_j and initial angle of rotation α_j . Secondly, use the following ansatz for the excitation amplitudes $c_{i+(j-1)N_r} = c_j^{(m)} e^{im(\varphi_i + \alpha_j)}$ (with $i = 1..N_p$, and $j = 1..N_r$) and construct the matrix (31) for each m . Finally, solve the eigenvalue problem and obtain the spectrum $\{\tilde{\mathcal{E}}^{(m)}\}$ with eigenvectors of excitation eigenstates $\{c_j^{(m)}\}$

Let us denote the probability amplitudes for a single excitation by two subindices $c_{i+(j-1)N_r}$. The first subindex enumerates the emitters of a certain ring $i = 1..N_p$ as in Section 2.1, while the second subindex corresponds to the ring with $j = 1..N_r$. To calculate the single excitation spectrum, we use equation (9) with the ansatz similar to (18):

$$c_{i+(j-1)N_r} = c_j^{(m)} e^{im(\varphi_i + \alpha_j)}, \quad j = 1..N_r \quad (30)$$

where $\varphi_i = (i - 1)2\pi/N_p$, α_j is the initial angle of rotation of the j -th ring in xy plane, and $c_j^{(m)}$ is the excitation amplitude describing the j -th ring in an eigenstate with quasi-momentum m [see figure 7]. A ket-vector for the corresponding eigenstate is written as $|\psi^{(m)}\rangle = \sum_{j=1}^{N_r} \sum_{i=1}^{N_p} c_{i+(j-1)N_r} |e_{i+(j-1)N_r}\rangle$.

As we can notice, a key difference from a single ring case is N_r unknown amplitudes $\{c_j^{(m)}\}_{j=1}^{N_r}$ instead of one for a certain value of m . After inserting this new ansatz in (9) and employing the ring dipole sums defined in equation (21), we obtain a system of equations to find N_r right eigenstates of (5) with the quasi-

momentum m as:

$$\underbrace{\begin{pmatrix} \tilde{\varepsilon}_1^{(m)} & \tilde{\chi}_{1,2}^{(m)} & \tilde{\chi}_{1,3}^{(m)} & \cdots & \tilde{\chi}_{1,N_r}^{(m)} \\ \tilde{\chi}_{2,1}^{(m)} & \tilde{\varepsilon}_2^{(m)} & \tilde{\chi}_{3,2}^{(m)} & \cdots & \tilde{\chi}_{2,N_r}^{(m)} \\ \vdots & \vdots & \vdots & \ddots & \vdots \\ \tilde{\chi}_{1,N_r}^{(m)} & \tilde{\chi}_{2,N_r}^{(m)} & \tilde{\chi}_{3,N_r}^{(m)} & \cdots & \tilde{\varepsilon}_{N_r}^{(m)} \end{pmatrix}}_{M^{(m)}} \begin{pmatrix} c_1^{(m)} \\ c_2^{(m)} \\ \vdots \\ c_{N_r}^{(m)} \end{pmatrix} = \tilde{\mathcal{E}}^{(m)} \begin{pmatrix} c_1^{(m)} \\ c_2^{(m)} \\ \vdots \\ c_{N_r}^{(m)} \end{pmatrix}, \quad (31)$$

where the diagonal entries of the introduced matrix are defined according to (20) and (21) as $\tilde{\varepsilon}_j^{(m)} = -\frac{i}{2} - \frac{3}{4}\Sigma^{(m)}(R_j, N_p)$, the energies of the excitation located only at j -th ring without the interaction with other rings. The non-diagonal entries are defined as normalized inter-ring coupling strengths

$$\tilde{\chi}_{j,l} = -\frac{3\pi c}{\omega_0} e^{im(\alpha_l - \alpha_j)} \sum_{n=1}^{N_p} e^{im\varphi_n} G_{zz}(|\mathbf{r}_{1+(j-1)N_r} - \mathbf{r}_{n+(l-1)N_r}|, \omega_0). \quad (32)$$

For the definition of G_{zz} see equation (16). In order to denote the eigenvalues of the multi-ring structure, we use the letter \mathcal{E} instead of ε . It will be useful further to distinguish the eigenvalues of multi-ring structures from the eigenvalues (20) of a single ring.

A general scheme for the efficient diagonalization of equation (9) for multi-ring structures is illustrated in figure 30. After this, we obtain a set of N_r eigenvalues and eigenstates for each m . In section 3.2, eigenvalue problem (31) will be solved analytically for $N_r = 2$ rings and will be demonstrated that the interaction between two states with the same m leads to the formation of subradiant states with a larger Q-factor.

To sum up, in order to calculate a single excitation spectrum of N_r concentric rings, namely $N = N_r \times N_p$ states with all possible values of angular quasi-momentum, one needs to diagonalize $N_r \times N_r$ matrix for each positive m instead of the diagonalization of $N \times N$ matrix representing the total Hamiltonian (3).

2.6 Doubly excited eigenstates

In sections 2.1 and 2.5, equations for calculating the single excitation spectrum of ring structures, namely (9) and (31), are formulated and investigated. This section is devoted to the analysis of the double excitation spectrum when states of a system are described by ket-vector (10). In this case, the study becomes more

complicated than for a single excitation case due to a significant dimensionality growth from N to $N(N - 1)/2$ for N emitters. However, in order to gain an understanding of doubly excited states with the angular quasi-momentum, one can formulate a general approach to obtain a double excitation spectrum illustrated by a relatively simple example of a ring of $N = N_p = 6$ emitters shown in figure 4.

As well as for singly excited eigenstates, the doubly excited eigenstates of a ring can be distinguished by the angular quasi-momentum m taking the same values as for a single excitation case [see section 2.1]. Hence, the double excitation amplitudes can be connected to each other by a relationship similar to (18). Thus, the whole set of double excitation amplitudes can be reduced to a set of “independent” amplitudes that differ not only by a phase factor $e^{im\varphi'}$ but also differ in absolute value. Here m is the state angular quasi-momentum, n is an integer and $\varphi' = 2\pi/N_p$.

Let us first consider an example of a ring of $N_p = 6$ emitters [see figure 4]. As discussed in section 2.2, rotation of a ring by $\varphi' = 2\pi/N_p$ angle around z axis converts the double excitation amplitudes as $c_{ij} \rightarrow e^{im\varphi'} c_{i'j'}$ where $i' = (i + 1) \bmod N_p$ and $j' = (j + 1) \bmod N_p$ [see figure 6(a)]. Thus, taking into account the symmetry of amplitudes $c_{ij} = c_{ji}$ and their transformation upon the ring rotation, a whole set of $N_p(N_p - 1)/2 = 15$ amplitudes c_{ij} for a ring of $N_p = 6$ emitters is reduced to three following sets:

$$\begin{aligned} S_1 &= \{c_{12}, c_{23}, c_{34}, c_{45}, c_{56}, c_{16}\}; \\ S_2 &= \{c_{13}, c_{24}, c_{35}, c_{46}, c_{15}, c_{26}\}; \\ S_3 &= \{c_{14}, c_{25}, c_{36}\}. \end{aligned} \tag{33}$$

Note that $c_{23} = e^{im\varphi'} c_{12}$, $c_{34} = e^{im\varphi'} c_{23} = e^{i2m\varphi'} c_{12}$ for the first set S_1 ; $c_{24} = e^{im\varphi'} c_{13}$, $c_{35} = e^{im\varphi'} c_{24} = e^{i2m\varphi'} c_{13}$ for the second set S_2 , and so on [$\varphi' = \pi/3$].

Hence, the doubly excited eigenstates of a ring of six emitters are determined only by three amplitudes $\{c_{12}, c_{13}, c_{14}\}$, while the singly excited eigenstates in a ring are determined only by one amplitude c_1 (see section 2.1). Thus, the number of doubly excited eigenstates with a certain value of angular quasi-momentum m equals three or less for a ring of $N_p = 6$ emitters. In order to clarify the latter point,

let us note that $c_{14} = 0$ for values of $m = \pm 1$ and $m = 3$. Indeed, $c_{14} = e^{im\varphi'} c_{36}$, then $c_{14} = e^{i3m\varphi'} c_{14}$ or $c_{14} (e^{i3m\varphi'} - 1) = 0$ implies two possible cases:

- $e^{i3m\varphi'} - 1 = 0$, then $3m\varphi' = 2\pi n$ where n is integer. After inserting $\varphi' = \pi/3$, one can obtain that $m = 2n$ is an *even* integer number;
- otherwise, for odd $m = (2n + 1)$, the amplitude is $c_{14} = 0$.

Hence, it is proven that $c_{14} = c_{25} = c_{36} = 0$ for $m = \pm 1$ and $m = 3$ values of angular quasi-momentum.

Thus, one ring of six emitters supports $N_0 = 3$ doubly excited states with $m = 0$, $N_{+1} = 2$ states with $m = +1$, $N_{-1} = 2$ states with $m = -1$, $N_{+2} = 3$ states with $m = +2$, $N_{-2} = 3$ states with $m = -2$, and $N_3 = 2$ states with $m = 3$. The total number of states is $3 \times 2 + 3 \times 3 = 15$ for a ring of $N_p = 6$ emitters as it should be according to the formula $\frac{N_p(N_p-1)}{2}$.

After dividing the amplitudes into sets, we can derive the effective eigenvalue equations for doubly excited states similar to the single excitation case (31). Looking at Schrödinger equation for double excitation amplitudes (11), one can notice that the amplitude c_{ij} is coupled via Green's tensor (16) only to the amplitudes for which one of the indices $-i$ or j remains the same. Hence, the amplitude c_{12} is coupled only to c_{23} and c_{16} amplitudes from S_1 set; to c_{13} , c_{24} , c_{15} , and c_{26} amplitudes from S_2 set; and to c_{14} , and c_{25} amplitudes from S_3 set. Taking into account the phase relationship between the amplitudes for each set, one can write the equation for c_{12} :

$$\begin{aligned} \tilde{\varepsilon}^{(m)} c_{12} = & \left(-i + \tilde{g}_{13} e^{im\varphi'} + \tilde{g}_{26} e^{i5m\varphi'} \right) c_{12} \\ & + \left(\tilde{g}_{23} + \tilde{g}_{14} e^{im\varphi'} + \tilde{g}_{25} e^{i4m\varphi'} + \tilde{g}_{16} e^{i5m\varphi'} \right) c_{13} \\ & + \left(\tilde{g}_{24} + \tilde{g}_{15} e^{im\varphi'} \right) c_{14}, \end{aligned} \quad (34)$$

where $\tilde{g}_{ij}(\omega_0)$ is given by (4). In a similar way, we can write the equations for c_{13} and c_{14} amplitudes and obtain the eigenvalue equation for doubly excited states in a compact matrix form as follows:

$$\begin{pmatrix} M_{11} & M_{12} & M_{13} \\ M_{21} & M_{22} & M_{23} \\ M_{31} & M_{32} & M_{33} \end{pmatrix} \begin{pmatrix} c_{12} \\ c_{13} \\ c_{14} \end{pmatrix} = \tilde{\varepsilon}^{(m)} \begin{pmatrix} c_{12} \\ c_{13} \\ c_{14} \end{pmatrix}, \quad (35)$$

where

$$\begin{aligned}
M_{11} &= -\mathbf{i} + \tilde{g}_{13}\mathbf{e}^{im\varphi'} + \tilde{g}_{26}\mathbf{e}^{i5m\varphi'}, \\
M_{12} &= \tilde{g}_{23} + \tilde{g}_{14}\mathbf{e}^{im\varphi'} + \tilde{g}_{25}\mathbf{e}^{i4m\varphi'} + \tilde{g}_{16}\mathbf{e}^{i5m\varphi'}, \\
M_{13} &= \tilde{g}_{24} + \tilde{g}_{15}\mathbf{e}^{im\varphi'}, \\
M_{21} &= \tilde{g}_{23} + \tilde{g}_{12}\mathbf{e}^{im\varphi'} + \tilde{g}_{14}\mathbf{e}^{i2m\varphi'} + \tilde{g}_{36}\mathbf{e}^{i5m\varphi'}, \\
M_{22} &= -\mathbf{i} + \tilde{g}_{15}\mathbf{e}^{i2m\varphi'} + \tilde{g}_{35}\mathbf{e}^{i4m\varphi'}, \\
M_{23} &= \tilde{g}_{34} + \tilde{g}_{16}\mathbf{e}^{i2m\varphi'}, \\
M_{31} &= \tilde{g}_{24} + \tilde{g}_{13}\mathbf{e}^{i2m\varphi'} + \tilde{g}_{15}\mathbf{e}^{i3m\varphi'} + \tilde{g}_{46}\mathbf{e}^{i5m\varphi'}, \\
M_{32} &= \tilde{g}_{34} + \tilde{g}_{12}\mathbf{e}^{im\varphi'} + \tilde{g}_{16}\mathbf{e}^{i3m\varphi'} + \tilde{g}_{45}\mathbf{e}^{i4m\varphi'}, \\
M_{33} &= -\mathbf{i}
\end{aligned} \tag{36}$$

with $\varphi' = \pi/3$ being the angular separation for a ring of six emitters. Moreover, equation (35) can be used for $m = 0$ and $m = \pm 2$. However for $m = \pm 1$ and $m = 3$, it can be simplified to the following equation since $c_{14} = 0$ for these values of m :

$$\begin{pmatrix} M_{11} & M_{12} \\ M_{21} & M_{22} \end{pmatrix} \begin{pmatrix} c_{12} \\ c_{13} \end{pmatrix} = \tilde{\varepsilon}^{(m)} \begin{pmatrix} c_{12} \\ c_{13} \end{pmatrix}. \tag{37}$$

Equations (35) and (37) are used in section 3.1 for the calculation of the spectrum of doubly excited states and investigation of subradiant states in a ring of six emitters.

One can generalize this approach for a ring of N_p emitters. A set of $N_p(N_p - 1)/2$ double excitation amplitudes can be reduced for *even* N_p to $(N_p/2 - 1)$ sets of N_p doubly excited amplitudes each and one set of $N_p/2$ amplitudes as follows

$$\begin{aligned}
S_1 &= \{c_{12}, c_{23}, c_{34}, \dots, c_{N_p-1, N_p}, c_{N_p, 1}\}, \\
S_2 &= \{c_{13}, c_{24}, c_{35}, \dots, c_{N_p-1, 1}, c_{N_p, 2}\}, \\
&\vdots \\
S_{N_p/2-1} &= \{c_{1, N_p/2}, c_{2, N_p/2+1}, c_{3, N_p/2+2}, \dots, c_{N_p/2-2, N_p-1}, c_{N_p/2-1, N_p}\}, \\
S_{N_p/2} &= \{c_{1, N_p/2+1}, c_{2, N_p/2+2}, c_{3, N_p/2+3}, \dots, c_{N_p/2-1, N_p-1}, c_{N_p/2, N_p}\}.
\end{aligned} \tag{38}$$

Note that $c_{ij} = c_{ji}$. Moreover, the amplitudes in $S_{N_p/2}$ set equal to zero for odd m since a condition $\frac{N_p}{2}m\varphi' = 2\pi n$ should be satisfied for $S_{N_p/2}$ set because its dimension is not N_p but $N_p/2$ (see a proof above for $N_p = 6$).

For *odd* N_p , the amplitudes can be divided into the following $(N_p - 1)/2$ sets of N_p amplitudes:

$$\begin{aligned}
S_1 &= \{c_{12}, c_{23}, c_{34}, \dots, c_{N_p-1, N_p}, c_{N_p, 1}\}, \\
S_2 &= \{c_{13}, c_{24}, c_{35}, \dots, c_{N_p-1, 1}, c_{N_p, 2}\}, \\
&\vdots \\
S_{(N_p-1)/2} &= \{c_{1, (N_p+1)/2}, c_{2, (N_p+3)/2}, c_{3, (N_p+5)/2}, \dots, c_{N_p-1, (N_p-3)/2}, c_{N_p, (N_p-1)/2}\}.
\end{aligned} \tag{39}$$

The number of sets is equal to the number of doubly excited states N_m for each m in a ring of emitters. Figure 8 summarizes the values of N_m for different parities of angular quasi-momentum m and the number of emitters N_p in a ring. For arbitrary N_p , one can get equations similar to (35) using the same approach.

Number of states N_m (m is fixed)	N_p is even		N_p is odd	
	$\frac{N_p}{2}$ is even	$\frac{N_p}{2}$ is odd	$\frac{(N_p + 1)}{2}$ is even	$\frac{(N_p + 1)}{2}$ is odd
even m	$\frac{N_p}{2}$	$\frac{N_p}{2}$	$\frac{(N_p - 1)}{2}$	$\frac{(N_p - 1)}{2}$
odd m	$\frac{N_p}{2} - 1$	$\frac{N_p}{2} - 1$	$\frac{(N_p - 1)}{2}$	$\frac{(N_p - 1)}{2}$

Figure 8 – Number of doubly excited eigenstates N_m in a single ring of N_p emitters N_m for the fixed value of angular quasi-momentum m depending on the parity of m (rows) and N_p (columns)

Let us consider the most general case of N_r rings with the same number of emitters N_p . For simplicity, we first determine the number of doubly excited states N_m with each angular quasi-momentum m in $N_r = 2$ rings of $N_p = 6$ emitters [see figure 9]. First of all, two excitations can occupy one of the rings, being in a state with angular quasi-momentum m . The number of states with m for one ring N_m is given in figure 8. For two rings, we need to multiply this number by two.

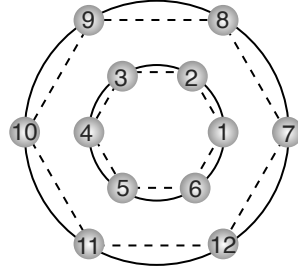


Figure 9 – Enumeration of emitters for $N_r = 2$ concentric rings of $N_p = 6$ emitters

For even m , there are six sets of amplitudes:

$$\begin{aligned}
S_1 &= \{c_{12}, c_{23}, c_{34}, c_{45}, c_{56}, c_{16}\} \\
S_2 &= \{c_{13}, c_{24}, c_{35}, c_{46}, c_{15}, c_{26}\}; \\
S_3 &= \{c_{14}, c_{25}, c_{36}\}; \\
S_4 &= \{c_{78}, c_{89}, c_{9,10}, c_{10,11}, c_{11,12}, c_{12,7}\}; \\
S_5 &= \{c_{79}, c_{8,10}, c_{9,11}, c_{10,12}, c_{11,7}, c_{12,8}\}; \\
S_6 &= \{c_{7,10}, c_{8,11}, c_{9,12}\}.
\end{aligned} \tag{40}$$

Thus, two rings support *at least* 6 doubly excited states with each even m ($m = 0, m = 2, m = -2$). For each odd m ($m = 1, m = -1, m = 3$), there are *at least* 4 states because the amplitudes in sets S_3 and S_5 are zero. However, these are not all possibilities for placing two excitations on two rings. A first excitation can also occupy the inner ring while the second one occupies the outer ring yielding to the following six sets of amplitudes and six states for each m :

$$\begin{aligned}
S_7 &= \{c_{17}, c_{28}, c_{39}, c_{4,10}, c_{5,11}, c_{12,6}\} \\
S_8 &= \{c_{18}, c_{29}, c_{3,10}, c_{4,11}, c_{5,12}, c_{67}\}; \\
S_9 &= \{c_{19}, c_{2,10}, c_{3,11}, c_{4,12}, c_{57}, c_{68}\}; \\
S_{10} &= \{c_{1,10}, c_{2,11}, c_{3,12}, c_{47}, c_{58}, c_{69}\}; \\
S_{11} &= \{c_{1,11}, c_{2,12}, c_{37}, c_{48}, c_{69}, c_{7,10}\}; \\
S_{12} &= \{c_{1,12}, c_{27}, c_{38}, c_{49}, c_{5,10}, c_{6,11}\}.
\end{aligned} \tag{41}$$

Thus, two rings of six emitters support 66 doubly excited states. In particular, $N_0 = 12$ doubly excited states with $m = 0$, $N_{+1} = 10$ states with $m = +1$,

$N_{-1} = 10$ states with $m = -1$, $N_{+2} = 12$ states with $m = +2$, $N_{-2} = 12$ states with $m = -2$, and $N_3 = 10$ states with $m = 3$.

Using a similar approach, we can find the number of doubly excited states N_m with a certain angular quasi-momentum m for *even* N_p as

$$N_m = \begin{cases} N_r \times \frac{N_p}{2} + \frac{N_r(N_r - 1)}{2} \times N_p & \text{even } m, \\ N_r \times \left(\frac{N_p}{2} - 1\right) + \frac{N_r(N_r - 1)}{2} \times N_p & \text{odd } m. \end{cases} \quad (42)$$

For *odd* N_p , the value of N_m is

$$N_m = N_r \times \frac{(N_p - 1)}{2} + \frac{N_r(N_r - 1)}{2} \times N_p \quad (43)$$

for even and odd m .

In this chapter, we considered singly and doubly excited eigenstates in ring structures of transverse emitters. Due to the rotational symmetry of the system, we can introduce the angular quasi-momentum m describing the phase shift between emitters. This helped us to reduce the dimensionality of the eigenvalue problem to N_r for a single-excitation manifold in N_r concentric rings of N_p emitters. For two excitations, the dimensionality is given by (42) for even N_p , and by (43) for odd N_p . Moreover, we studied the change of ring eigenstates under transformations from the symmetry group of the structure. We provided a correspondence between the value of m and irreducible representations of symmetry group C_{6v} for six emitters. The same approach can be applied to any number of emitters. The correspondence of the ring states to certain irreducible representations determines nonzero terms in the expansion of a doubly excited state over the products of singly excited states. It also strictly shows that the angular quasi-momentum of the doubly excited state is equal to the sum of the angular quasi-momentum of singly excited states.

3 SUBRADIANT EIGENSTATES OF RING OLIGOMERS

This chapter applies formalism developed in chapter 2 to model singly and doubly excited eigenstates of a single ring and ring oligomers. The main aim of the chapter is the investigation of subradiant eigenstates (with a large lifetime) and the mechanisms of their formation.

3.1 Subradiance of a small single ring

First of all, let us model singly and doubly excited eigenstates with various values of angular quasi-momentum m of a single ring of $N_p = 6$ identical emitters shown in figure 4. We recall that the obtained normalized and shifted complex eigenvalue of the eigenstate with m can be written as $\tilde{\varepsilon}^{(m)} = \left(\frac{\omega^{(m)} - \omega_0}{\gamma_0} \right) - i \frac{\gamma^{(m)}}{2\gamma_0}$ [see equation (6)]. The ratio $Q_0 = \frac{\omega_0}{\gamma_0}$ defines a quality factor (Q-factor) of a single emitter resonance. In order to characterize the resonances of collective states, one can introduce the collective Q-factor as $Q^{(m)} = \frac{\omega^{(m)}}{\gamma^{(m)}}$. In order to simplify the analysis, let us notice that the frequency detuning of collective state $|\omega^{(m)} - \omega_0| \ll \omega_0$ since $\omega_0 \ll \gamma_0$ for atomic resonances. Thus, one can define approximately a ratio of the collective state's Q-factor to the single emitter's Q-factor as $\frac{Q^{(m)}}{Q_0} \approx \left(\frac{\gamma_0}{\gamma^{(m)}} \right)^{-1}$. The latter ratio of decay rates can be extracted from analytically or numerically calculated eigenvalues as $\frac{\gamma^{(m)}}{\gamma_0} = -2 \text{Im}(\tilde{\varepsilon}^{(m)})$.

Figures 10(a) and 10(b) show the ratio of Q-factors $\frac{Q^{(m)}}{Q_0}$ for singly and doubly excited eigenstates, respectively, as functions of normalized separation between emitters a [see inset in figure 10(b)]. The eigenenergies for singly excited states are calculated using equation (20) with analytically derived dipole sum (22) whereas the spectrum of doubly excited states is calculated from equation (35) for even $m = 0, \pm 2$, and from equation (37) for odd $m = \pm 1, 3$. In figure 10(a) one can see that $\frac{Q^{(m)}}{Q_0} \lesssim 1$ for $m = 0$, $\frac{Q^{(m)}}{Q_0} \sim 1$ for $m = \pm 1$, and $\frac{Q^{(m)}}{Q_0} \gg 1$ for $m = \pm 2$ and $m = 3$ in the considered range of separations $a/\lambda_0 \lesssim 0.25$. The states with $\frac{Q^{(m)}}{Q_0} \ll 1$ are called superradiant (low-Q) states whereas the states with $\frac{Q^{(m)}}{Q_0} \gg 1$ are subradiant (high-Q) states.

We can see also in figure 10(a) that the larger m , the higher the Q-factor of the state. This can be explained as follows. A ring excitation in the state $|\psi^{(m)}\rangle$ can be

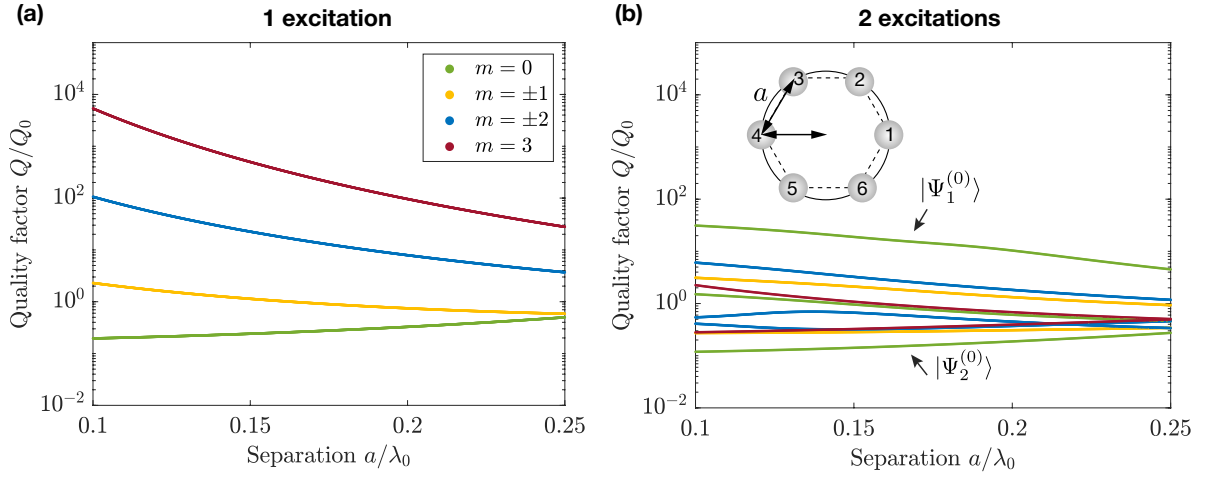


Figure 10 – (Logarithmic scale) Quality factors (Q-factors) of eigenstates in a ring of $N_p = 6$ as a function of separation between emitters normalized by the resonant wavelength of a single emitter resonance [see inset in (b)]. The curves in both subfigures are colored depending on the value of angular quasi-momentum m [see legend in (a)]. The emitters are polarized perpendicular to the ring plane. The collective Q-factor is normalized by that of a single emitter Q_0 . $Q/Q_0 = (-2 \text{Im}[\tilde{\varepsilon}])^{-1}$ where ε is calculated from (20) for singly excited states (a), and from (35) for doubly excited states (b) in a single ring. The dipole sums for a ring of six emitters are calculated in (22). Kets in (b) highlight doubly excited states with the highest and lowest Q-factor

considered as a quasi-particle with a wavenumber $\frac{k_m}{k_0} = \frac{m}{N_p a/\lambda_0}$ [25, 29]. Therefore, suppression of radiative losses of the states is due to a mismatch between k_m and wavenumber in free space k_0 and the former growth with m .

Moreover, if separation a/λ_0 decreases, Q-factors increase for $m \neq 0$ but the Q-factor of $m = 0$ eigenstate decreases [see figure 10(a)]. Note that the collective decay rates $\gamma^{(m)}$ approach the Dicke limit for $a/\lambda_0 \rightarrow 0$ [7]. In this limit, the separation between the emitters is so small that their interaction can be considered to be infinitely strong. This, in turn, for the case of N_p transverse dipoles leads to the appearance of $(N_p - 1)$ collective states with $\gamma = 0$ ($Q = \infty$), and one superradiant state with $\gamma = N_p \gamma_0$ ($Q = Q_0/N_p$). The first case of infinite Q-factors corresponds to $m \neq 0$ whereas the second case is the state with $m = 0$.

In accordance with figure 10(b), adding a second excitation to the ring can help to increase the Q-factors of states with a small quasi-momentum, namely $m = 0$ and $m = \pm 1$, by several orders of magnitude. Indeed, the state with $m = 0$ becomes the most subradiant for the case of two excitations. This state is

denoted as $|\Psi_1^{(0)}\rangle$ in figure 10(b). It is also interesting to compare $|\Psi_1^{(0)}\rangle$ with the most superradiant state, also with $m = 0$, denoted as $|\Psi_2^{(0)}\rangle$ in figure 10(b).

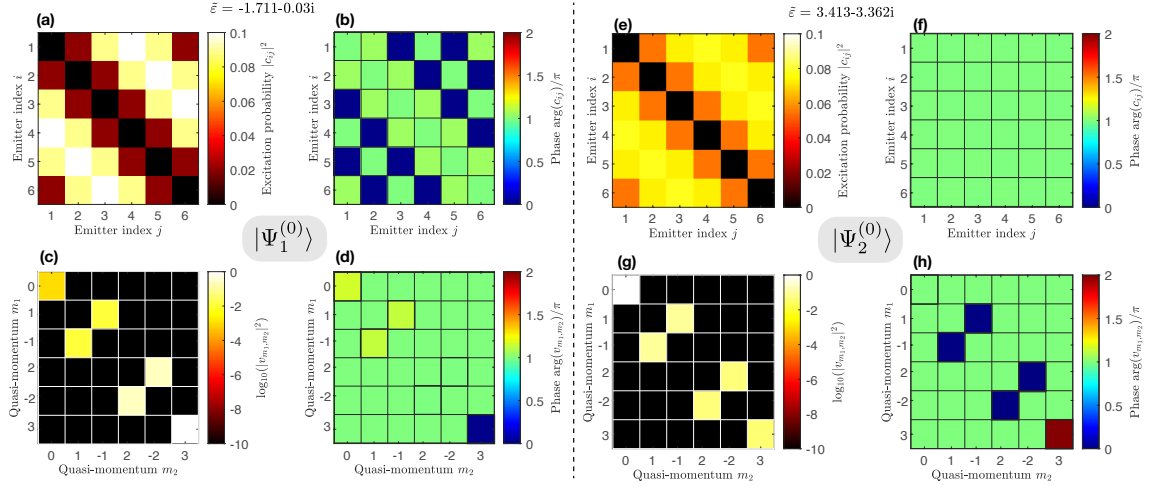


Figure 11 – Maps for doubly excited states with $m = 0$ from figure 10(b) with the highest and lowest Q-factor (the corresponding eigenvalues are written on top of the figure). The ring is composed of $N_p = 6$ emitters separated by $a/\lambda_0 = 0.16$. (a) Probabilities $|c_{ij}|^2$ of the double excitation of i -th and j -th emitter. Note that $c_{ii} = 0$ but $c_{ji} = c_{ij}$. (b) The phase of amplitudes c_{ij} in units of π . (c, d) Coefficients $\{v_{m_1, m_2}\}$ of expansion of doubly excited state over the products of singly excited states with angular quasi-momentum m_1 and m_2 (28). The coefficients are calculated using the method described in section 2.3. The absolute values of v_{m_1, m_2} are shown in (c), and their phases in units of π are shown in (d). There are only nonzero coefficients such that $(m_1 + m_2) \bmod 6 = 0$. (e-h) The same but for low-Q state $|\Psi_2^{(0)}\rangle$

Figures 11(a)-(d) and 11(e)-(h) contain all the information about $|\Psi_1^{(0)}\rangle$ and $|\Psi_2^{(0)}\rangle$ states for $a/\lambda_0 = 0.16$, respectively. Figures 11(c) and 11(g) show the expansion coefficients v_{m_1, m_2} of doubly excited states $|\Psi_1^{(0)}\rangle$ and $|\Psi_2^{(0)}\rangle$ over the products of singly excited states $|\psi^{(m_1)}\rangle |\psi^{(m_2)}\rangle$ [see section 2.3]. One can see that subradiant singly excited states with $m_1 = m_2 = 3$ mostly contribute to subradiant $|\Psi_1^{(0)}\rangle$ [see figures 10(a) and 11(c)] whereas the highest contribution to superradiant $|\Psi_2^{(0)}\rangle$ is given by $m_1 = m_2 = 0$ term with the highest radiative losses [see figures 10(a) and 11(g)]. Note that in figures 11(c) and 11(g) $v_{m_1, m_2} \neq 0$ such that $(m_1 + m_2) = 0 \pmod 6$.

Thus, it is possible to reach higher Q-factors for low m by going from a single excitation manifold to a double excitation one. Nevertheless, the Q-factor

of the most subradiant singly excited state is higher than the Q-factor of the most subradiant doubly excited state.

In the next section, we introduce a general approach for obtaining high-Q states for all values m in single and double excitation manifolds based on the coupling of modes in two subsystems with the same symmetry.

3.2 Mechanism of subradiant state formation

We consider an oligomer consisting of two open subsystems of emitters (A and B). We denote the initial singly excited states of subsystems without interaction (\hat{H}_0) as $|\varphi_a\rangle$ and $|\varphi_b\rangle$ with complex eigenenergies read as $\tilde{\varepsilon}_s \equiv \left(\frac{\omega_s - \omega_0}{\gamma_0} - i \frac{\gamma_s}{\gamma_0} \right)$ where $s = a, b$. Assume that $|\varphi_a\rangle$ and $|\varphi_b\rangle$ have the same symmetry, i.e. enter the same irreducible representation. Now let us introduce the interaction between the states through the continuum of free space modes (radiation continuum) \hat{V} depending on the system's parameters. One can formally write down the 2×2 Hamiltonian describing the whole system as

$$\hat{H} = \underbrace{\begin{pmatrix} \tilde{\varepsilon}_a & 0 \\ 0 & \tilde{\varepsilon}_b \end{pmatrix}}_{\hat{H}_0} + \underbrace{\begin{pmatrix} 0 & \tilde{\chi}_{ab} \\ \tilde{\chi}_{ba} & 0 \end{pmatrix}}_{\hat{V}}, \quad (44)$$

where $\tilde{\chi}_{ab}$ and $\tilde{\chi}_{ba}$ are the coupling strengths. The eigenenergies of “dressed” eigenstates of \hat{H} can be easily found as

$$\tilde{\mathcal{E}}_{\pm} = \frac{1}{2} \left[\tilde{\varepsilon}_a + \tilde{\varepsilon}_b \pm \sqrt{(\tilde{\varepsilon}_a - \tilde{\varepsilon}_b)^2 + 4\tilde{\chi}_{ab}\tilde{\chi}_{ba}} \right]. \quad (45)$$

The corresponding “dressed” eigenstates are

$$|\psi_{\pm}\rangle \equiv \begin{pmatrix} u_{\pm} \\ v_{\pm} \end{pmatrix} = \frac{1}{\sqrt{1 + |\eta_{\pm}|^2}} \begin{pmatrix} 1 \\ \eta_{\pm} \end{pmatrix}, \quad (46)$$

where

$$\eta_{\pm} = -\frac{1}{2\tilde{\chi}_{ab}} \left[\tilde{\varepsilon}_a - \tilde{\varepsilon}_b \mp \sqrt{(\tilde{\varepsilon}_a - \tilde{\varepsilon}_b)^2 + 4\tilde{\chi}_{ab}\tilde{\chi}_{ba}} \right]. \quad (47)$$

As shown further, the radiative decay rate of a “dressed” state $\gamma_{-} \propto \text{Im} \left[\tilde{\mathcal{E}}_{-} \right]$ can be significantly decreased compared to that of a single emitter and single rings

due to destructive interference of $|\varphi_s\rangle$ states (subsystems A and B) in radiation to the continuum.

3.3 An example of $m = 0$ with a central emitter

First, let us consider a simple example of the formation of a high-Q state with $m = 0$ via the mechanism (44) in an oligomer of emitters. Figure 12(a) presents an oligomer composed of a ring of N_p emitters and one emitter placed at the ring center coinciding with the origin of Cartesian coordinate systems. A total number of singly excited eigenstates, in this case, is $N = N_p + 1$.

Note that a central emitter can interact only with the ring state having $m = 0$. Indeed, the electric field strength of the state (26) with $m \neq 0$ is zero at the ring center due to a symmetry reason (see also figure 14), therefore, a coupling strength of the state field with an emitter placed at the field zero is $\varkappa \propto \mathbf{d} \cdot \mathbf{E}^* = 0$.

For the considered ensemble, it is natural to choose the initial states as the excited state of a central emitter, $|\varphi_a\rangle = |e\rangle$, and the ring eigenstate with $m = 0$, $|\varphi_b\rangle = |\psi_{\text{ring}}^{(0)}\rangle$ [see equation (26)]. The state $|e\rangle$ obviously has $m = 0$. On this basis, the entries of the Hamiltonian (44) are an excited emitter energy $\tilde{\varepsilon}_a = -\frac{i}{2}$, an excited ring energy $\tilde{\varepsilon}_b = -\frac{i}{2} - \frac{3}{4}\Sigma^{(0)}(R, N_p)$, $\tilde{\varkappa}_{ba} = -\frac{3\pi c}{\omega_0}G_{zz}(R, \omega_0)$, and $\tilde{\varkappa}_{ab} = N_p \varkappa_{ba}$ [see equations (4), (9), and (20)].

According to (45), these parameters yield the following eigenenergies for the ‘‘dressed’’ oligomer states with $m = 0$:

$$\tilde{\mathcal{E}}_{\pm} = -\frac{i}{2} - \frac{3}{8}\Sigma^{(0)}(R, N_p) \pm \frac{3}{4}\Delta, \quad (48)$$

where $\Delta = \sqrt{\frac{1}{4}[\Sigma^{(0)}(R, N_p)]^2 + N_p \left[\frac{4\pi c}{\omega_0}G_{zz}(R, \omega_0)\right]^2}$ is a complex energy gap between the states. The corresponding eigenstates of the oligomer with $m = 0$ read as

$$|\psi_{\pm}\rangle = u_{\pm}|g\rangle^{\otimes N_p} \otimes |e\rangle + v_{\pm}|\psi_{\text{ring}}^{(0)}\rangle \otimes |g\rangle, \quad (49)$$

where $|u_+|^2 + |v_+|^2 = |u_-|^2 + |v_-|^2 = 1$. Note that the other $(N_p - 1)$ states of the oligomer with $m \neq 0$ are $|\psi_{\text{ring}}^{(m)}\rangle \otimes |g\rangle$ where $|\psi_{\text{ring}}^{(m)}\rangle$ is a state (26).

One can also find η_{\pm} for the considered oligomer from equation (47) and substitute it into equation (46) to obtain u_{\pm} and v_{\pm} excitation amplitudes. Their physical meaning is the following: $\frac{1}{\sqrt{N_p}}v_{\pm}e^{im\varphi_i}$ is the excitation amplitude of an

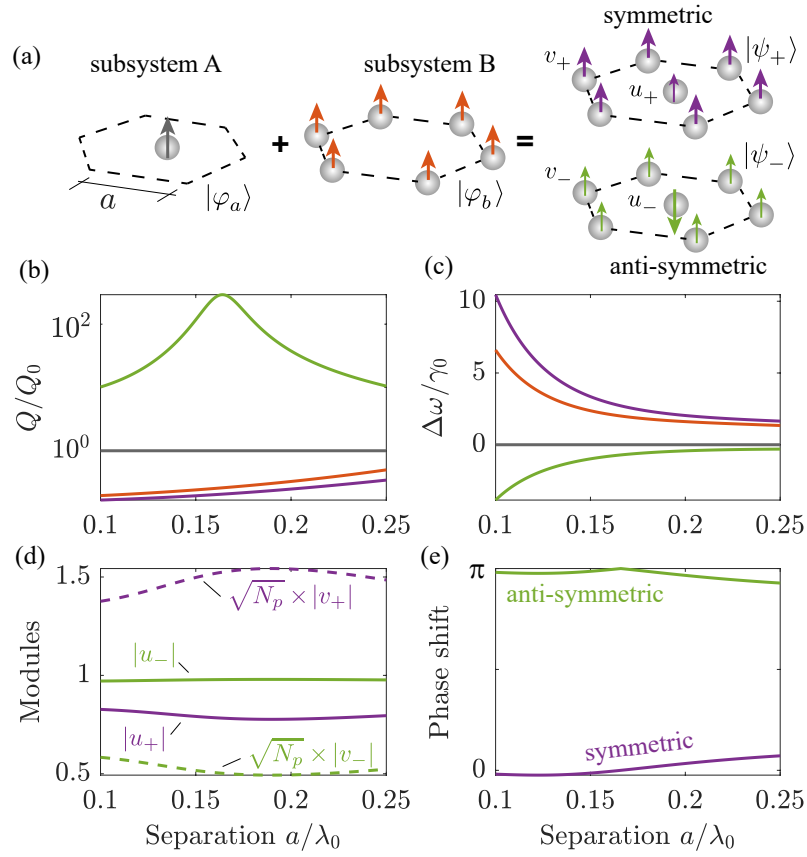


Figure 12 – *High-Q singly excited state with $m = 0$.* (a) Illustration of mechanism (44) of the high-Q state formation in oligomer composed of a central emitter (subsystem A) and a ring (subsystem B). The oligomer supports symmetric and anti-symmetric (high-Q) states (49). (b) (Logarithmic scale) Dependence of normalized Q-factor of states shown in (a) on the separation between emitters a/λ_0 . The collective Q-factor is calculated as $Q/Q_0 = (-2 \text{Im}[\mu])^{-1}$ where $\mu = -i/2$ for a central emitter (gray), μ is given by eq. (20) with $m = 0$ for the ring state (orange), μ is given by eq. (48) for anti-symmetric (green) and symmetric (violet) states. (c) The frequency detuning of the states, $\frac{\Delta\omega}{\gamma_0} \equiv \frac{\omega - \omega_0}{\gamma_0} = \text{Re}[\mu]$. (d) The absolute values of excitation amplitudes of a ring (v_{\pm}) and central emitter (u_{\pm}) for symmetric and anti-symmetric states (49). (e) The phase shifts for amplitudes are defined as $\arg(u_+) - \arg(v_+)$ (violet) and $\arg(u_+) - \arg(v_-)$ (green)

emitter in a ring, and u_{\pm} is the excitation amplitude of a central emitter [see figure 12(a)]. Moreover, the phase shift between u_- and v_- is close to π whereas that is almost zero for u_+ and v_+ [see figure 12(e) for $N_p = 6$]. Hence, the “+” (resp. “-”) subscript corresponds to a symmetric (resp. an anti-symmetric) state $|\psi_+^{(0)}\rangle$ (resp. $|\psi_-^{(0)}\rangle$) shown in figure 12(a).

Figures 12(c) and 12(b) show the normalized Q-factors and frequency detunings of initial $|\varphi_s^{(0)}\rangle$, and oligomer $|\psi_{\pm}^{(0)}\rangle$ states for $N_p = 6$. One can see

the frequency and Q-factor of the symmetric state approach those of a single ring because excitation is mostly localized at the ring rather than at a central emitter $\frac{|u_+|}{\sqrt{N_p|v_+|}} \lesssim 2$ [see figure 12(d)]. At the same time, the frequency of the anti-symmetric state approaches the frequency of a single emitter with the increase of a because $\frac{|u_-|}{\sqrt{N_p|v_-|}} \gtrsim 2$. However, the Q-factor of the anti-symmetric state is remarkably higher than Q_0 and has a maximum $Q/Q_0 = 292$ around $a/\lambda_0 = 0.16$ when the phase shift between probability amplitudes of ring and emitter excitations equals to π exactly [see figure 12(e)]. This can be explained by the fact that the radiative losses of dipole emitters are proportional to a square of the mean dipole moment which is strongly reduced compared to that of a single dipole at $a/\lambda_0 = 0.16$ [see figure 12(d)]. Thus, an anti-symmetric state is subradiant for the considered range of separations $a/\lambda_0 \lesssim 0.25$ while a symmetric state is a superradiant one. Moreover, the Q-factor for the anti-symmetric state tends to infinity in the Dicke limit ($a/\lambda_0 \rightarrow 0$) while the Q-factor for the symmetric state approaches $1/N$.

To conclude, we can notice that an inner subsystem (central emitter) is most excited in an anti-symmetric, high-Q state while an excitation prefers to occupy an outer subsystem (ring) in a symmetric state. A similar situation takes place for subradiant singly excited and doubly excited states in two-ring structures.

3.4 Subradiant states with non-zero angular quasi-momentum

The ensemble composed of the ring with a central emitter shown in figure 12 supports a high-Q state with angular quasi-momentum $m = 0$. However, this ensemble can not be applied to obtain subradiant states with $m \neq 0$ because a central emitter can not interact with the ring states with $m \neq 0$. It motivates us to consider a different ensemble composed of two concentric rings shown in the inset of figure 13(b). The rings have the same number of emitters N_p but different radii R_1 and $R_2 > R_1$. The total number of emitters is $N = 2N_p$. As the initial states $|\varphi_a^{(m)}\rangle$ and $|\varphi_b^{(m)}\rangle$, we choose the singly excited eigenstates with the same angular quasi-momentum m in single rings (26) of radius R_1 and R_2 , respectively. Note that the states (26) enter the orthogonal irreducible representations for different angular quasi-momentum m , therefore the states of two rings can interact only if they have the same m .

In this case, the Hamiltonian (44) matches the matrix (31) for two rings. As written under (31), $\tilde{\varepsilon}_a^{(m)}$ and $\tilde{\varepsilon}_b^{(m)}$ are the energies of an excitation occupying one

of two non-interacting rings [see equation (20)]. For clarity, we write again the expressions for $\tilde{\varepsilon}_a^{(m)}$ and $\tilde{\varepsilon}_b^{(m)}$:

$$\tilde{\varepsilon}_a^{(m)} = -\frac{i}{2} - \frac{3}{4}\Sigma^{(m)}(R_1, N_p), \quad \tilde{\varepsilon}_b^{(m)} = -\frac{i}{2} - \frac{3}{4}\Sigma^{(m)}(R_2, N_p). \quad (50)$$

The coupling between rings is symmetric [$\tilde{\varkappa}_{ab}^{(m)} = \tilde{\varkappa}_{ba}^{(m)}$ in (44)] and given by (32). Inserting (50) and (32) into (45), we obtain the eigenenergies $\tilde{\mathcal{E}}_{\pm}^{(m)}$ of the states with angular quasi-momentum m in a two-ring oligomer. The corresponding eigenstates of a two-ring oligomer simply read as:

$$\left| \psi_{\pm}^{(m)} \right\rangle = u_{\pm} \underbrace{\left| \varphi_a^{(m)} \right\rangle}_{1^{\text{st}} \text{ ring}} \otimes \underbrace{\left| g \right\rangle^{\otimes N_p}}_{2^{\text{nd}} \text{ ring}} + v_{\pm} \underbrace{\left| g \right\rangle^{\otimes N_p}}_{1^{\text{st}} \text{ ring}} \otimes \underbrace{\left| \varphi_b^{(m)} \right\rangle}_{2^{\text{nd}} \text{ ring}}. \quad (51)$$

As well as for the case of a ring and a central emitter, the interaction between two subsystems (rings here) leads to the formation of anti-symmetric, high-Q states but for all values of angular quasi-momentum m as illustrated in figure 13(a). For a two-ring structure, $\frac{1}{\sqrt{N_p}}u_{\pm}^{(m)}e^{im\varphi_i}$ and $\frac{1}{\sqrt{N_p}}v_{\pm}^{(m)}e^{im\varphi_i}$ have a meaning of the excitation amplitudes of the i -th emitter in the first and second ring, respectively, within a symmetric or anti-symmetric state. Note that $|u_+^{(m)}| < |v_+^{(m)}|$ for the symmetric state, and $|u_-^{(m)}| > |v_-^{(m)}|$ for the anti-symmetric state similar to the case of a ring with a central emitter.

Figures 13(b-c) demonstrate Q-factors for the eigenstates (51) for two rings of $N_p = 6$ emitters. For all values of angular quasi-momentum m , we can observe a good enhancement of the Q-factor for a two-ring oligomer by several orders of magnitude compared to that for two single, non-interacting rings. We can also see the peaks of the Q-factor whose positions depend on the m and are essentially governed by the ratio of ring radii R_2/R_1 [the latter is covered in more detail in the next section]. The origin of maxima in the Q-factor, as before, is associated with the optimal conditions for the destructive interference (phase shift is π) of two emitter subsystems. Moreover, we show in section 3.7 that this interference leads to the suppression of low-order radiant multipoles (vector spherical harmonics). The radiation into the far field of high-Q states is associated with high-order multipoles (hexapoles, 32-poles) although we consider ensembles with pure dipole response.

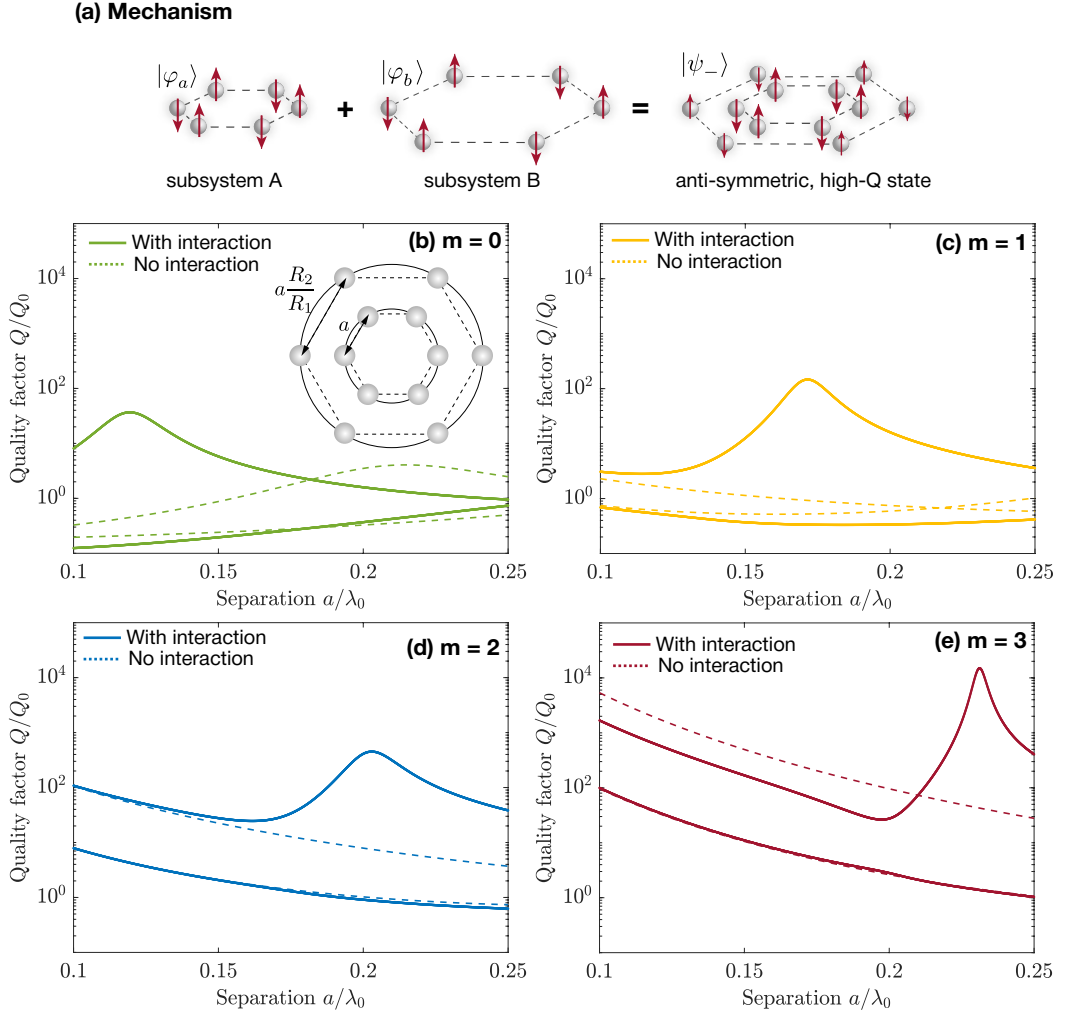


Figure 13 – *High-Q, singly excited states with different angular quasi-momentum m in two-ring oligomer.* (a) Mechanism of the formation of the high-Q state governed by the Hamiltonian (44). The mechanism is shown for $m = 3$. An excitation mostly occupies an inner ring. (b-d) (Logarithmic scale) Dependence of Q-factors of rings' states with different m on the separation between emitters a for $R_2/R_1 = 2$ [see inset in (a)]. The collective Q-factor is calculated as $Q/Q_0 = (-2 \text{Im}[\mu])^{-1}$. The dashed lines show the Q-factors of the states of non-interacting rings [$\mu = \text{eq. (50)}$] while the solid lines are for interacting rings [$\mu = \text{eq. (45)}$ with $\tilde{\varepsilon} = \text{eq. (50)}$ and $\tilde{\varkappa} = \text{eq. (32)}$]

Note that Q-factors in figure 13 approach the Dicke limit at small separations between emitters as described in section 3.1. The symmetric state with $m = 0$ has $\frac{Q}{Q_0} = \frac{1}{N}$ while other $(N - 1)$ states have $\frac{Q}{Q_0} = \infty$ in Dicke limit.

The high-Q states allow us to obtain a good enhancement of the field component E_z , transverse to the structure, in the near field wave zone $z \lesssim \lambda_0$. The electric

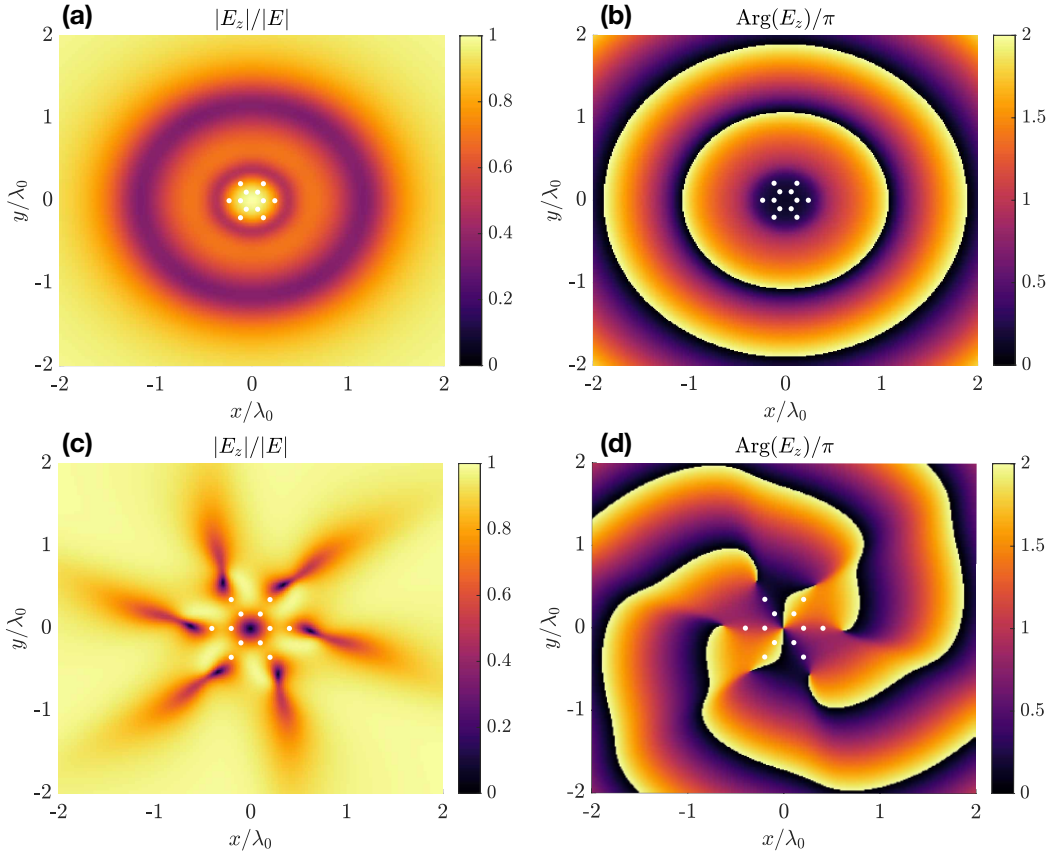


Figure 14 – *Magnitude and phase distributions of electric field component E_z generated by high- Q states of two-ring oligomer in $z/\lambda_0 = 0.5$ plane. The oligomer is shown in figure 13 with $R_2/R_1 = 2$. The electric field is calculated by equation (52). (a,c) The magnitude of E_z normalized by that of the total electric field for high- Q states with angular quasi-momentum (a) $m = 0$, and (b) $m = 1$. The separation between the rings a/λ_0 is picked such that the states have a maximum of Q -factor in figures 13(b), and 13(c), respectively. The white dots indicate the positions of emitters in the $z = 0$ plane just for clarity. (b,d) The phase of E_z in units of π for the states with (b) $m = 0$, and (d) $m = 1$*

field of a collection of electric dipoles can be written via Green's tensor (16) as

$$\mathbf{E}(\mathbf{r}, \omega_0) = \frac{\omega_0^2}{c^2 \epsilon_0} \sum_{i=1}^N \hat{\mathbf{G}}_0(\mathbf{r} - \mathbf{r}_i, \omega_0) \mathbf{d}_i, \quad (52)$$

where $\{\mathbf{r}_i\}_{i=1}^N$ is a set of coordinates of dipoles. In a semi-classical approach, we can assign a classical dipole moment to i -th emitter by a simple rule $\mathbf{d}_i = \mathbf{d} \times c_i$ where c_i is the excitation amplitude within a singly excited eigenstate, and \mathbf{d} is the emitter transition dipole moment as before.

Figure (14) shows the amplitude and the phase of E_z generated by high- Q states with $m = 0$ and $m = 1$ in two rings with a/λ_0 such that Q -factors of the

states have maxima in figures 13(c) and 13(d). One can see that the states demonstrate remarkably different field profiles. The field of $m = 0$ state in figure 14(a) has an axial symmetry with maxima and minima of the field due to the interference of fields generated by rings. Moreover, the field phase for $m = 0$ continuously varies from 0 to 2π along a radial direction [see figure 14(b)]. For $m = 1$, a non-zero angular quasi-momentum manifests itself as a vortex for the field strength and the phase [see figures 14(c) and 14(d)]. Moreover, the state with $m = 1$ has zero field at the center of rings whereas the state with $m = 0$ has a field maxima at this point.

3.5 Doubly excited subradiant states

The discussed above physical mechanism based on the interaction of two emitter subsystems can be applied to obtaining subradiance of doubly excited states with non-zero angular momentum. A two-ring structure shown in figure 13 has two independent parameters such as the ratio of ring radii R_2/R_1 , and separation between emitters a/λ_0 . Since a singly excited state with $m = 3$ has the highest Q-factor among all singly excited states in a two-ring oligomer [see figure 13], let us maximize the Q-factor of a doubly excited state with $m = 3$ by varying R_2/R_1 and a/λ_0 . Figure 15 shows the Q-factor of the most subradiant doubly excited state with $m = 3$ calculated for two rings by equation (11) taking into account the symmetry of the states as discussed in section 2.6. One can see an enhancement of Q by two orders of magnitude compared to Q_0 for $R_2/R_1 = 2.2$ and $a/\lambda_0 = 0.16$.

In order to interpret obtained optimal parameters, let us model doubly excited eigenstates with $m = 3$, $|\Psi^{(m)}\rangle = \sum_{i=1}^N \sum_{j=i+1}^N c_{ij} |e_i e_j\rangle$ where $|e_i e_j\rangle = \hat{\sigma}_i^\dagger \hat{\sigma}_j^\dagger |g\rangle^{\otimes N}$. We recall that double excitation amplitudes obey the Pauli principle $c_{ii} = 0$, and reciprocity $c_{ij} = c_{ji}$ [see section 1.3]. As discussed in section 2.3, a doubly excited state can be expanded into a sum of products of singly excited states $|\Psi^{(m)}\rangle = \sum_{m_1, m_2} v_{m_1, m_2} |\psi^{(m_1)}\rangle |\psi^{(m_2)}\rangle$ where $v_{m_1, m_2} \neq 0$ for $m_1 + m_2 = m \pmod{N_p}$ where N_p is the number of emitters per ring. Figure 16 shows maps with amplitudes c_{ij} and v_{m_1, m_2} of four doubly excited states $|\Psi_s^{(3)}\rangle$ with $m = 3$ in a two-ring oligomer with optimal parameters $R_2/R_1 = 2.2$ and $a/\lambda_0 = 0.16$. The states should be analyzed together since they have the same symmetry, i.e. enter the same irreducible representation of the C_{6v} group. As written in

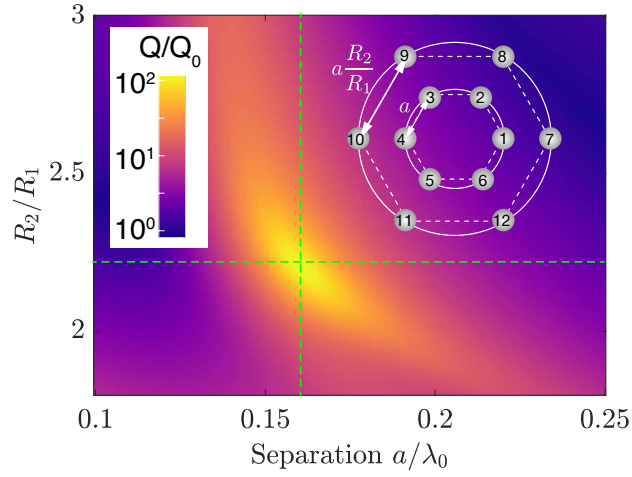


Figure 15 – Q-factor of $\left| \Psi_1^{(3)} \right\rangle$ the subradiant doubly excited state with angular quasi-momentum $m = 3$ as function of R_2/R_1 and a/λ_0 . The collective Q-factor is normalized by the Q-factor of a single emitter resonance Q_0 . The inset shows two rings of six emitters with the enumeration of emitters

section 2.5, the states with $m = 3$ are transformed by one-dimensional irreducible representations. Obviously, the states presented in figure 16 cannot enter A_1 and A_2 representations because these representations preserve the state under rotations [see figure 6(c)]. Indeed, let us take a look at the maps with absolute values and phases of amplitudes c_{ij} , for example, in figures 16(a) and 16(b) for $\left| \Psi_1^{(3)} \right\rangle$ state. As shown in figure 6(a), a rotation of rings by $\pi/3$ angle around z -axis permutes the indices so that non-zero amplitude c_{23} corresponds to amplitude c_{12} before the rotation. Since the state has $m = 3$, then $c_{23} = c_{12}e^{im\pi/3} = -c_{12}$ as illustrated figures 16(a) and 16(b). Thus, the states in figure 16 can enter B_1 or B_2 irreducible representations [see figure 6(c)]. In order to finally identify, let us consider the symmetry of the states under reflection with respect to the axis intersecting the emitters [σ_d in figure 6(b)]. After this reflection, $c_{12} \rightarrow c_{16}$. From figure 16(b), we can find that $c_{16} = -c_{12}$, therefore the state is anti-symmetric with respect to σ_d and enters B_1 irreducible representation [see figure 6(c)]. It can be shown that other states $\left| \Psi_2^{(3)} \right\rangle$, $\left| \Psi_3^{(3)} \right\rangle$, and $\left| \Psi_4^{(3)} \right\rangle$ also enter the same representation B_1 . Note that two rings have ten doubly excited eigenstates with $m = 3$ [see (42)]. The discussed here eigenstates enter B_1 irreducible representation, while the other six states enter different representation B_2 and consequently do not interact with these four due to having different symmetry.

Figure 16 also shows the eigenvalues $\tilde{\mathcal{E}}_s^{(3)}$ of doubly excited states with $m = 3$ for $R_2/R_1 = 2.2$ and $a/\lambda_0 = 0.16$. The state $\left| \Psi_1^{(3)} \right\rangle$ is subradiant

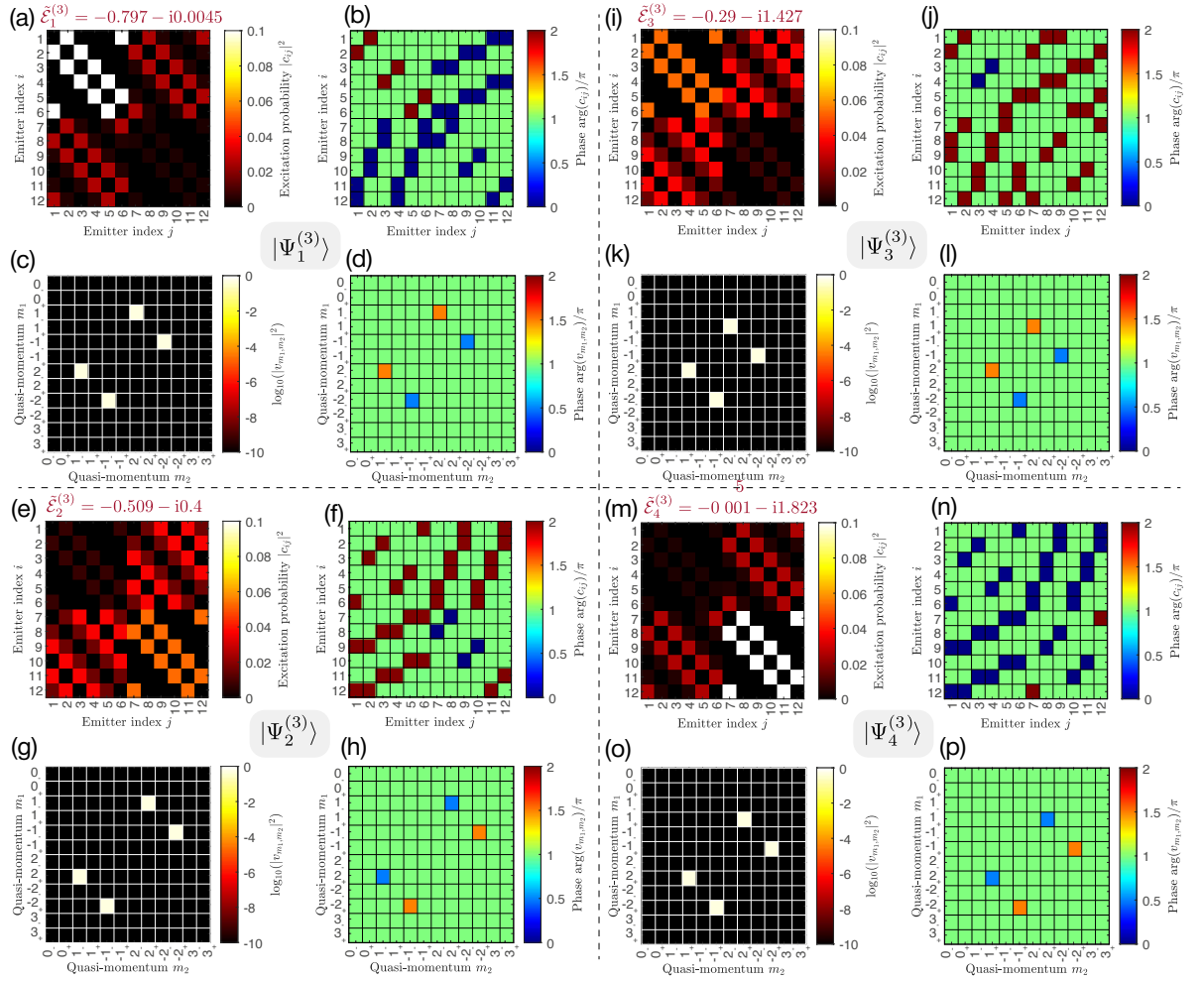


Figure 16 – Maps of excitation amplitudes c_{ij} and expansion coefficients v_{m_1, m_2} for doubly excited states with $m = 3$ in two rings $|\Psi_s^{(3)}\rangle$ where $s = 1, 2, 3, 4$ [see equation (53)]. The rings of six emitters have $R_2/R_1 = 2.2$ and $a/\lambda_0 = 0.16$ corresponding to the maximum of Q-factor in figure 15. $\tilde{\mathcal{E}}_s$ are the eigenvalues (54) of shown states for these parameters of rings. The indices i and j enumerate the emitters such that a set of indices $\{1, 2, \dots, 6\}$ is for the inner ring (ring A), and $\{7, 8, \dots, 12\}$ is for the outer ring (ring B) as shown in figure 15. The indices m_1 and m_2 denote the angular quasi-momentum of singly excited states with the subscript \pm corresponding to symmetric or anti-symmetric state (51)

with $Q/Q_0 = (-2 \text{Im}[\tilde{\mathcal{E}}])^{-1} \approx 110$. There are also one radiant state $|\Psi_2^{(3)}\rangle$ with $Q/Q_0 \approx 1.25$, and two superradiant states $|\Psi_3^{(3)}\rangle$, $|\Psi_4^{(3)}\rangle$ with $Q/Q_0 \approx 0.35$ and $Q/Q_0 \approx 0.27$, respectively. As well as for the singly excited states in two rings, the most subradiant doubly excited state $|\Psi_1^{(3)}\rangle$ is mostly localized on the inner ring rather than on two rings or on the outer ring [see figure 17(a)] while, for the most radiant state $|\Psi_4^{(3)}\rangle$, excitations occupy an outer ring. The states with intermediate losses $|\Psi_2^{(3)}\rangle$ and $|\Psi_3^{(3)}\rangle$ are localized between the rings. Using expansions over

products of singly excited states in figures 16, we can write doubly excited states ordered by increasing radiative losses as

$$\begin{aligned}
|\Psi_1^{(3)}\rangle &= \frac{i}{\sqrt{2}} \left(|\psi_-^{(+1)}\rangle |\psi_-^{(+2)}\rangle + |\psi_-^{(+2)}\rangle |\psi_-^{(+1)}\rangle \right) \\
&\quad - \frac{i}{\sqrt{2}} \left(|\psi_-^{(-1)}\rangle |\psi_-^{(-2)}\rangle + |\psi_-^{(-2)}\rangle |\psi_-^{(-1)}\rangle \right), \\
|\Psi_2^{(3)}\rangle &= \frac{i}{\sqrt{2}} \left(|\psi_-^{(+1)}\rangle |\psi_+^{(+2)}\rangle + |\psi_+^{(+2)}\rangle |\psi_-^{(+1)}\rangle \right) \\
&\quad - \frac{i}{\sqrt{2}} \left(|\psi_-^{(-1)}\rangle |\psi_+^{(-2)}\rangle + |\psi_+^{(-2)}\rangle |\psi_-^{(-1)}\rangle \right), \\
|\Psi_3^{(3)}\rangle &= \frac{i}{\sqrt{2}} \left(|\psi_+^{(+1)}\rangle |\psi_-^{(+2)}\rangle + |\psi_-^{(+2)}\rangle |\psi_+^{(+1)}\rangle \right) \\
&\quad - \frac{i}{\sqrt{2}} \left(|\psi_+^{(-1)}\rangle |\psi_-^{(-2)}\rangle + |\psi_-^{(-2)}\rangle |\psi_+^{(-1)}\rangle \right), \\
|\Psi_4^{(3)}\rangle &= \frac{i}{\sqrt{2}} \left(|\psi_+^{(+1)}\rangle |\psi_+^{(+2)}\rangle + |\psi_+^{(+2)}\rangle |\psi_+^{(+1)}\rangle \right) \\
&\quad - \frac{i}{\sqrt{2}} \left(|\psi_+^{(-1)}\rangle |\psi_+^{(-2)}\rangle + |\psi_+^{(-2)}\rangle |\psi_+^{(-1)}\rangle \right),
\end{aligned} \tag{53}$$

where $|\psi_{\pm}^{(m)}\rangle$ is symmetric/anti-symmetric singly excited states of a two-ring oligomer (51). Thus, doubly excited states (53) are composed of products of singly excited states with only $m_1 = \pm 1$ and $m_2 = \pm 2$. It is interesting to note that there are no contributions of products of singly excited states with $m_1 = 0$ and $m_2 = 3$ although $m_1 + m_2 = m = 3$. This can be easily understood by analyzing the products of irreducible representations of the C_{6v} symmetry group (29). The irreducible representation B_1 of states (53) only enters expansion of product $E_1 \times E_2$ corresponding to singly excited states with $m = \pm 1$ and $m = \pm 2$. However, the product of irreducible representations $A_1 \times B_2$ for states with $m = 0$ and $m = 3$ equals a different irreducible representation B_2 .

Acting with the Hamiltonian (3) on the states (53), we obtain the following expressions for the energies of doubly excited states via the energies of singly

excited states in two rings:

$$\begin{aligned}
\tilde{\mathcal{E}}_1^{(3)} &= \tilde{\mathcal{E}}_-^{(1)} + \tilde{\mathcal{E}}_-^{(2)}, \\
\tilde{\mathcal{E}}_2^{(3)} &= \tilde{\mathcal{E}}_-^{(1)} + \tilde{\mathcal{E}}_+^{(2)}, \\
\tilde{\mathcal{E}}_3^{(3)} &= \tilde{\mathcal{E}}_+^{(1)} + \tilde{\mathcal{E}}_-^{(2)}, \\
\tilde{\mathcal{E}}_4^{(3)} &= \tilde{\mathcal{E}}_+^{(1)} + \tilde{\mathcal{E}}_+^{(2)}.
\end{aligned} \tag{54}$$

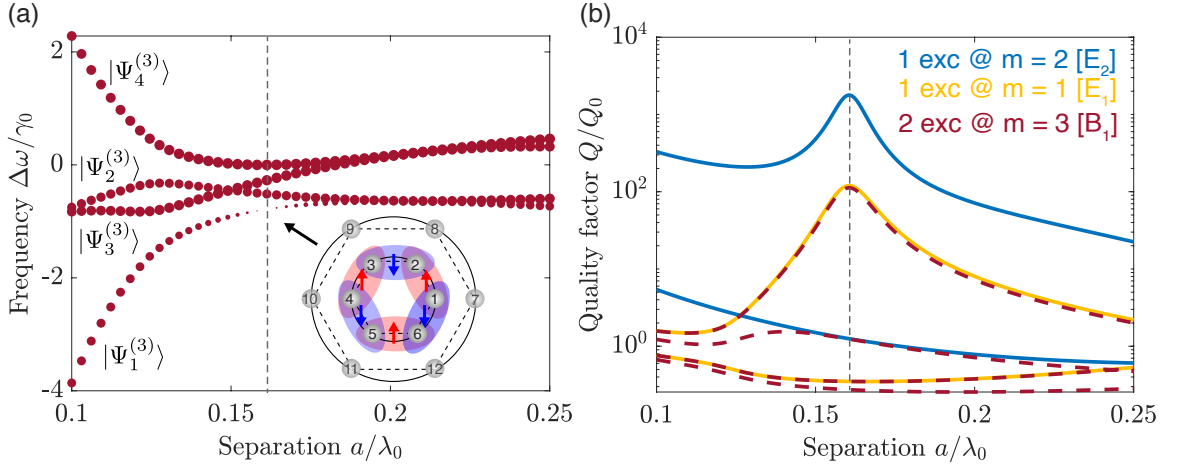


Figure 17 – (a) Frequency detuning $\frac{\Delta\omega}{\gamma_0} \equiv \frac{\omega_s - \omega_0}{\gamma_0} = \text{Re}[\tilde{\mathcal{E}}_s]$ of doubly excited states in two rings (53) with $m = 3$ for $R_2/R_1 = 2.2$. The dot size is proportional to the decay rate $\frac{\gamma_s}{\gamma_0} = -2 \text{Im}[\tilde{\mathcal{E}}_s]$ where $\tilde{\mathcal{E}}_s$ is given by eq. (54). The inset schematically

shows the largest amplitudes c_{ij} for doubly excited state $|\Psi_1^{(3)}\rangle$ obtained from figures 16(a,b). (b) Q-factors of doubly excited states (53) with $m = 3$ (burgundy dashed curves), singly excited states (51) with $m = 1$ (orange solid curves), and $m = 2$ (blue solid curves). Q-factors are calculated via the corresponding decay rates $Q/Q_0 \approx \gamma_0/\gamma$ since $\Delta\omega \ll \omega_0$

Now we can explain the maximum of the Q-factor of the state $|\Psi_1^{(3)}\rangle$ in figure 15 for parameters $R_2/R_1 = 2.2$ and $a/\lambda_0 = 0.16$ of two rings. Figure 17(a) shows the frequency detuning of doubly excited states by dots of size proportional to the decay rate of the state. Figure 17(b) shows the Q-factors for doubly excited states (53) with $m = 3$ and singly excited states (51) with $m = 1$ and $m = 2$. Since the energy (54) of the considered doubly excited states $|\Psi_1^{(3)}\rangle$ is just the sum of energies of subradiant singly excited states with $m = 1$ and $m = 2$, then the decay rates of these states are connected as follows $\gamma_1^{(3)} = \gamma_-^{(1)} + \gamma_-^{(2)}$. Hence, the Q-factor of the doubly excited state $Q_1^{(3)}$, such that $\frac{1}{Q_1^{(3)}} = \frac{1}{Q_-^{(1)}} + \frac{1}{Q_-^{(2)}}$, has

the maximum because the Q-factors of singly excited states $Q_-^{(1)}$, $Q_-^{(2)}$ also have maxima at $a/\lambda_0 = 0.16$ [see figure 17(b)].

We want to draw attention to the fact that one ring also supports a doubly excited state with $m = 3$, such that its irreducible representation is B_1 and its energy is the sum of energies of singly excited states in one ring with $m = 1$ and $m = 2$: $\tilde{\varepsilon} = \tilde{\varepsilon}^{(1)} + \tilde{\varepsilon}^{(2)}$ where $\tilde{\varepsilon}^{(m)}$ given by (20) for one ring. However, the Q-factor of this state is relatively small $Q^{(3)}/Q_0 \sim 1$ as shown in figure 10(b) because $Q^{(3)} \approx Q^{(1)}$ in one ring whereas $Q^{(1)}/Q_0 \sim 1$ as shown in figure 10(a). If we add a second ring to the system, the singly excited states with $m = 1$ in two rings can be anti-symmetric or symmetric $Q^{(1)} \rightarrow Q_-^{(1)}, Q_+^{(1)}$. The anti-symmetric state has a large Q-factor $Q_-^{(1)}/Q_0 \gg 1$, therefore, the doubly excited in two rings $|\Psi_1^{(3)}\rangle$ such that $Q^{(3)} \approx Q_-^{(1)}$ also has a large Q-factor. Thus, the interaction between two rings decreases the radiative losses of the states in both singly- and two-excitation manifolds.

3.6 Far-field radiation patterns of singly excited states

This section studies radiation patterns of the singly excited, high-Q states with $m = 1$ and $m = 2$ shown in figure 17(b). The total power radiated in the far field wave zone $r \gg \lambda_0$ by a dipole ensemble can be written through the time-averaged Poynting vector $\langle \mathbf{S} \rangle$ as

$$P = \int_{4\pi} r^2 \langle \mathbf{S} \rangle \cdot \mathbf{n} \, d\Omega. \quad (55)$$

The integration is carried out over a total solid angle $\int_{4\pi} d\Omega = \int_0^{2\pi} d\varphi \int_0^\pi d\theta \sin \theta$ for a sphere of radius $r \gg \lambda$ and center at the origin of the Cartesian coordinate system. $\mathbf{n} = (\cos \theta \cos \varphi, \cos \theta \sin \varphi, \sin \theta)$ is a unit vector normal to this spherical surface. The spherical angles θ and φ are defined according to figure 18(a). Let us introduce $p(\theta, \varphi) = r^2 \langle \mathbf{S} \rangle \cdot \mathbf{n}$ as a power radiated into a unite solid angle $d\Omega$ given by unite vector \mathbf{n} as shown in figure 18(a). $p(\theta, \varphi)$ determines a radiation pattern of the system and depends on a radial component of $\langle \mathbf{S} \rangle = \frac{1}{2} \text{Re} (\mathbf{E}_{\text{FF}} \times \mathbf{H}_{\text{FF}}^*)$ where only far-field terms of generated electric \mathbf{E}_{FF} and magnetic \mathbf{H}_{FF} fields contribute to the outgoing radiation. For an electric dipole, $\mathbf{H}_{\text{FF}} = c\epsilon_0 \mathbf{n} \times \mathbf{E}_{\text{FF}}$ [44]. Moreover, \mathbf{E}_{FF} , \mathbf{H}_{FF} , and \mathbf{n} are orthogonal to each other in the far field $r \gg \lambda_0$ [see figure 18(a)], then $\langle \mathbf{S} \rangle = \frac{1}{2} c\epsilon_0 |\mathbf{E}_{\text{FF}}|^2 \mathbf{n}$ is always oriented along \mathbf{n} .

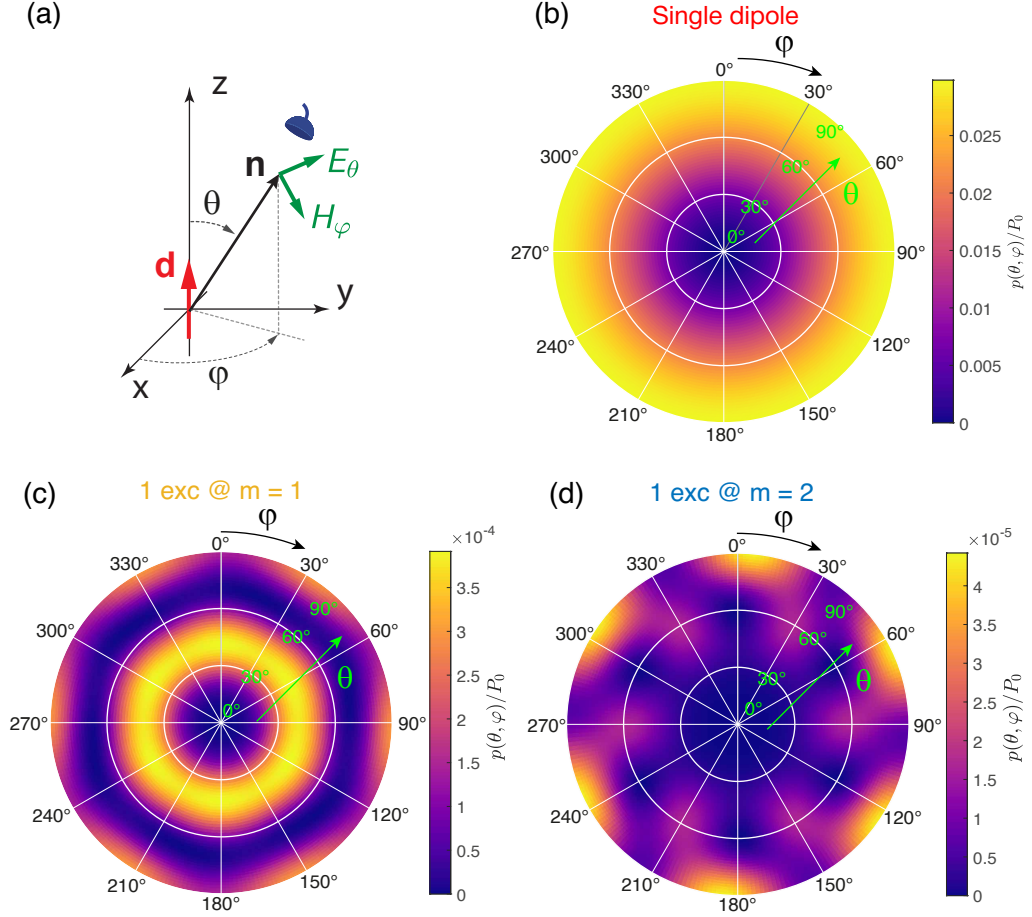


Figure 18 – (a) Scheme with the coordinates system for calculating angular dependence of far-field radiation. The green arrows show components of electric E_θ and magnetic H_φ far fields of a single dipole polarized along z -axis (red arrow). (b) Normalized radiation pattern (57) for a single oscillating dipole along z . (c,d) Normalized radiation patterns (57) for high-Q states with $m = 1$ and $m = 2$ from figure 17(b). The rings have $R_2/R_1 = 2.2$ and $a/\lambda_0 = 0.16$ when both states have the highest Q-factor in figure 17(b). In diagrams (b-d), θ angle is plotted along the radial direction and φ is along the angular direction. Note that the radiation patterns are symmetric with respect to the exchange $\theta \rightarrow \pi - \theta$ since the structures are placed in the xy plane

In order to calculate \mathbf{E}_{FF} from equation (52), we write down the far field Green's function $\hat{\mathbf{G}}_0(\mathbf{r} - \mathbf{r}_i, \omega_0)$ [see (16)]:

$$\hat{\mathbf{G}}_0^{\text{FF}}(\mathbf{r} - \mathbf{r}_i, \omega_0) = \frac{e^{ik_0 r - ik_0 \mathbf{n} \cdot \mathbf{r}_i}}{4\pi r} \left(\hat{\mathbf{I}} - \mathbf{n} \otimes \mathbf{n} \right), \quad (56)$$

where $\mathbf{n} \equiv \mathbf{r}/r$. In order to obtain this, we used $|\mathbf{r} - \mathbf{r}_i| \approx r - \mathbf{r} \cdot \mathbf{r}_i/r = r - \mathbf{n} \cdot \mathbf{r}_i$. Hence, the electric far field can be expressed as $\mathbf{E}_{\text{FF}} = \frac{e^{ik_0 r}}{r} \mathbf{f}(\mathbf{n})$ where $\mathbf{f}(\mathbf{n}) = -\frac{\omega_0^2}{c^2 \epsilon_0} \frac{\sin \theta}{4\pi} \sum_{i=1}^N e^{-ik_0 \mathbf{n} \cdot \mathbf{r}_i} \mathbf{d}_i$ is the scattering amplitude for dipole emitters polar-

ized in z -direction $\mathbf{d}_i = \mathbf{d} \times \mathbf{c}_i$. Thus, the radiation pattern is fully determined by the scattering amplitude $p(\theta, \varphi) = \frac{1}{2}c\epsilon_0 |\mathbf{f}(\mathbf{n})|^2$ and does not depend on the sphere radius r . For the obtained dipole scattering amplitude $\mathbf{f}(\mathbf{n})$, the radiation pattern of a dipole ensemble is finally written as

$$p(\theta, \varphi) = P_0 \times \frac{3}{32\pi} \sin^2 \theta \left| \sum_{i=1}^N e^{-ik_0 \mathbf{n} \cdot \mathbf{r}_i} \mathbf{c}_i \right|^2, \quad (57)$$

where $P_0 = \hbar\omega_0 \times \gamma_0$ is a total radiated power by a single dipole with γ_0 given by (2):

$$P_0 = \frac{\omega_0^4 |\mathbf{d}|^2}{3\pi c^3 \epsilon_0}. \quad (58)$$

Note that P_0 does not contain the Planck constant in its denominator in contrast to the decay rate γ_0 because P_0 can be derived in classical electrodynamics while γ_0 has a quantum origin.

Figure 18(b) shows the radiation pattern for a single dipole along z -axis [see figure 18(a)] calculated from equation (57), $p(\vartheta, \varphi)/P_0 \propto \sin^2 \theta$. Figures 18(c) and 18(d) show the radiation patterns for anti-symmetric, singly excited eigenstates with $m = 1$ and $m = 2$, respectively, from figure 17(b) when the states experience maxima of Q-factor. Note that the radiation patterns presented in figures 18(b-d) are symmetric with respect to the exchange $\theta \rightarrow \pi - \theta$ since the structures are placed in the xy plane. One can see a strong modification of the states' radiation patterns relative to a single dipole radiation pattern. The state with $m = 1$ also radiates into $\theta \in [\pi/6, \pi/3]$ and $\theta \in [2\pi/3, 5\pi/6]$ ranges for any φ . The state with $m = 2$ mostly radiates into $\theta \approx \pi/2$ as a single dipole at the angles $\varphi_i = (i-1)\pi/3$ of emitters' angles while the radiation pattern exhibits a "vortex". The maximum of $p(\theta, \varphi)/P_0$ for states with $m = 1$ and $m = 2$ is approximately one and two orders of magnitude smaller than for a single dipole.

3.7 Multipole expansion

A complicated view of the radiation patterns in figures 18(c) and 18(d) can be justified by a quite reach multipole content of the scattered field (52). In order to perform the multipole expansion of the radiated field, let us introduce electric

\mathbf{N} and magnetic \mathbf{M} vector spherical harmonics (VSH) [48]:

$$\begin{aligned}\mathbf{M}_{j,n}^{(s)}(\mathbf{r}, \omega) &= \nabla \times \left[\mathbf{r} z_j^{(s)}(kr) Y_{j,n}(\theta, \varphi) \right], \\ \mathbf{N}_{j,n}^{(s)}(\mathbf{r}, \omega) &= \frac{c}{\omega} \nabla \times \mathbf{M}_{j,n}^{(s)}(\mathbf{r}, \omega),\end{aligned}\quad (59)$$

where ∇ is the nabla operator, j is a total angular momentum ($j = 1$ - dipole, $j = 2$ - quadrupole, $j = 3$ - octupole, and so on), n is the projection of j on z -axis, $Y_{j,n}(\theta, \varphi)$ is a scalar spherical harmonics ($\propto e^{in\varphi}$). The superscript (s) takes values $s = 1$ or $s = 3$ such that $z_j^{(1)}(kr) \equiv j_j(kr)$ is the spherical Bessel function of order j , $z_j^{(3)}(kr) \equiv h_j(kr)$ is the first-kind spherical Hankel function of order j .

Free-space Green's function (16) can be expressed via VSHs as

$$\begin{aligned}\hat{\mathbf{G}}_0(\mathbf{r} - \mathbf{r}', \omega) &= -\frac{\mathbf{e}_r \otimes \mathbf{e}_r}{k^2} \delta(\mathbf{r} - \mathbf{r}') + ik \sum_{j=1}^{+\infty} \sum_{n=-j}^{+j} \frac{1}{j(j+1)} \times \\ &\begin{cases} \mathbf{M}_{j,n}^{(1)}(\mathbf{r}, \omega) \otimes \mathbf{M}_{j,-n}^{(3)}(\mathbf{r}', \omega) + \mathbf{N}_{j,n}^{(1)}(\mathbf{r}, \omega) \otimes \mathbf{N}_{j,-n}^{(3)}(\mathbf{r}', \omega), & \text{if } r > r', \\ \mathbf{M}_{j,n}^{(3)}(\mathbf{r}, \omega) \otimes \mathbf{M}_{j,-n}^{(1)}(\mathbf{r}', \omega) + \mathbf{N}_{j,n}^{(3)}(\mathbf{r}, \omega) \otimes \mathbf{N}_{j,-n}^{(1)}(\mathbf{r}', \omega), & \text{if } r < r', \end{cases}\end{aligned}\quad (60)$$

where $k = \omega/c$, \otimes is the dyadic product between two vectors, \mathbf{e}_r is the unit vector of radial direction.

In the far field, the distance between a field calculation point and the dipoles' coordinate is very large $r \gg r_i$, hence we need to choose the first option for the expansion of Green's function. Inserting (60) in (52), we obtain the following VSH expansion of the far field radiated by dipoles:

$$\mathbf{E}(\mathbf{r}, \omega_0) = \frac{\omega_0^3}{c^3 \epsilon_0} \sum_{j=1}^{+\infty} \sum_{n=-j}^{+j} \sum_{i=1}^N \left(a_{j,n}^{(i)} \frac{i \mathbf{N}_{j,n}^{(1)}(\mathbf{r}, \omega_0)}{\sqrt{j(j+1)}} + b_{j,n}^{(i)} \frac{i \mathbf{M}_{j,n}^{(1)}(\mathbf{r}, \omega_0)}{\sqrt{j(j+1)}} \right), \quad (61)$$

where the expansion coefficients are

$$\begin{aligned}a_{j,n}^{(i)} &= \frac{1}{\sqrt{j(j+1)}} \mathbf{N}_{j,-n}^{(3)}(\mathbf{r}_i, \omega) \cdot \mathbf{d}_i, \\ b_{j,n}^{(i)} &= \frac{1}{\sqrt{j(j+1)}} \mathbf{M}_{j,-n}^{(3)}(\mathbf{r}_i, \omega) \cdot \mathbf{d}_i.\end{aligned}\quad (62)$$

Let us insert (61) in (55). Taking into account the orthogonality conditions between VSHs and emitter identity (recall that $\mathbf{d}_i = \mathbf{d} \times \mathbf{c}_i$), integration in (55)

can be evaluated that leads to the following expression for a total radiated power normalized by (58):

$$\frac{P}{P_0} = \frac{3}{2} \sum_{j=1}^{+\infty} \sum_{n=-j}^{+j} \left(|a_{j,n}|^2 + |b_{j,n}|^2 \right), \quad (63)$$

where $a_{j,n} = \sum_{i=1}^N a_{j,n}^{(i)}$, $b_{j,n} = \sum_{i=1}^N b_{j,n}^{(i)}$. In order to obtain (63), we need to calculate the integrals like $\int r^2 [\mathbf{N} \times \mathbf{M}] \cdot \mathbf{n} \, d\Omega \propto k_0^{-2}$.

Let us draw a few conclusions about equation (63). First of all, it equals the ratio of decay rates, $\frac{P}{P_0} = \frac{\gamma}{\gamma_0}$ since $P = \hbar\omega_0 \times \gamma$ for one excitation stored in the ensemble. Secondly, $|a_{j,n}|^2$ and $|b_{j,n}|^2$ quantities show the contribution of electric and magnetic VSH with (j,n) to the radiation. Thirdly, all the VSHs contribute to the radiation independently because the interference terms like $a_{j,n}^* b_{j,n}$, $b_{j,n}^* a_{j,n}$ are absent in (63). This is in agreement with the equation for the scattered power of a single particle of spherical shape within Mie theory [49].

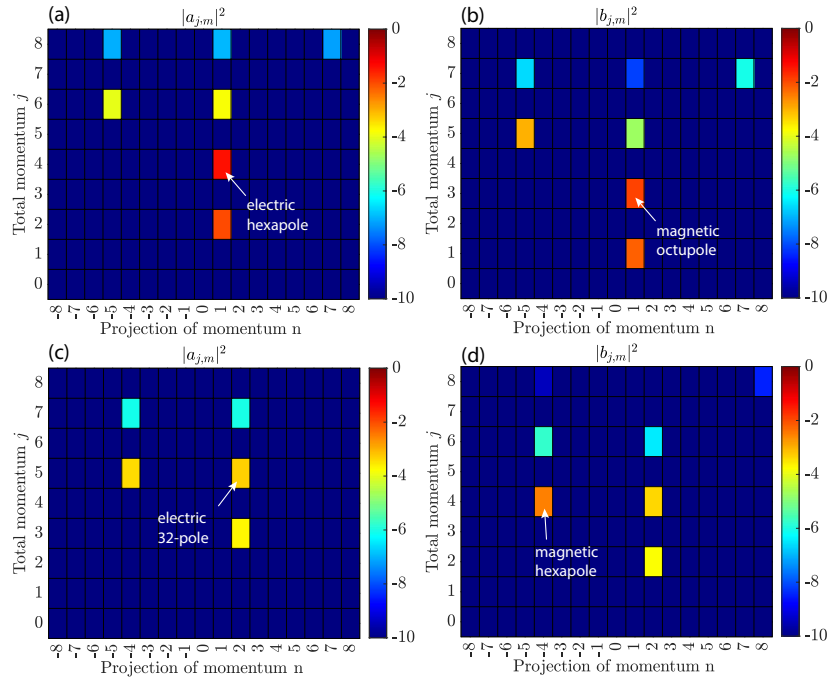


Figure 19 – Multipole expansion (63) for high-Q singly excited states with (a,b) $m = 1$ and (c, d) $m = 2$ of two rings. The ring radii are $R_2/R_1 = 2.2$ and the separation between emitters is $a/\lambda_0 = 0.16$ corresponding to maxima of Q-factors of the states in figure 17(b). The coefficients are calculated by equation (62) and presented on a logarithmic scale. The multipoles (VSHs) providing dominant contributions are highlighted

Figures 19(a,b) and figures 19(c,d) show the multipole contributions of VSHs to the radiated power for the subradiant, singly-excited states with $m = 1$ and $m = 2$, respectively. One can see that only the VSHs with $n \bmod 6 = m$ contribute to the radiation because the symmetry of the VSH should coincide with the symmetry of the state according to (62). The interference between different multipoles leads to complicated radiation patterns in figure 18. The subradiant properties of the states are due to the fact that the low-order multipoles are almost suppressed, while the main contribution to the radiation is given by higher-order multipoles. It is known that the higher the order of the multipole, the lower the amount of radiated power. One can see in figures 19(a,b) that the electric hexapole and magnetic octupole mainly contribute to the state with $m = 1$. As shown in figure 17(b), the state with $m = 2$ has a higher Q-factor than the state with $m = 1$ since the higher-order multipoles (electric 32-pole, and magnetic hexapole) mainly contribute to this state [see figures 19(c,d)].

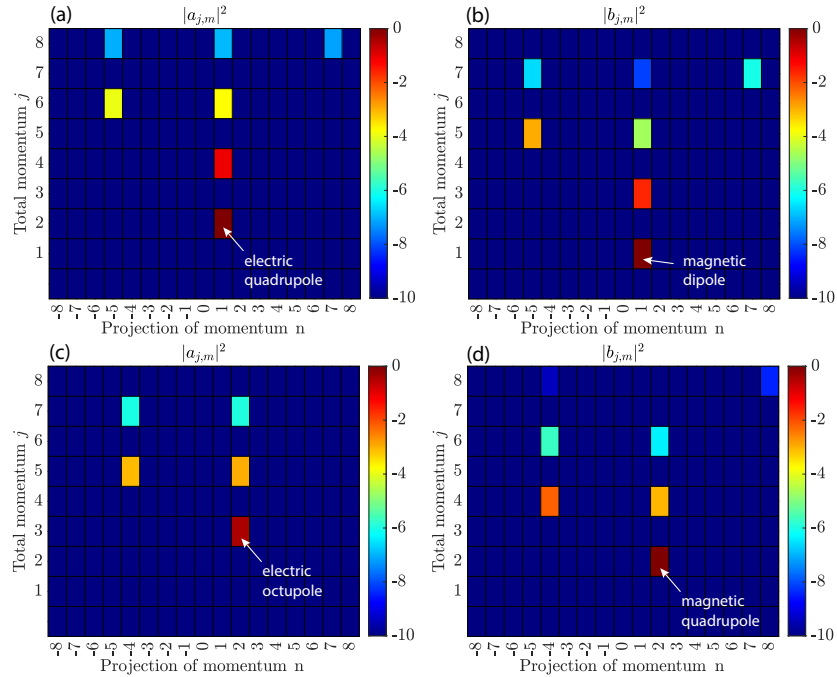


Figure 20 – The same as in figure 19 but the excitation amplitudes of rings $u_-^{(m)}$ and $v_-^{(m)}$ are assumed to be in phase

Suppression of high-order multipoles for high-Q states in the two-ring structure can be justified by a presence of π phase shift between the excitation amplitudes $u_-^{(m)}$ and $v_-^{(m)}$ of the rings. Figure 20 shows the multipole expansion for the states when two rings are in a phase that corresponds to the symmetric states. In this case, the symmetric states can be approximated in the far field by two radiat-

ing multipoles such as an electric quadrupole and a magnetic dipole for the state with $m = 1$, an electric octupole and magnetic quadrupole for the state with $m = 2$. The decrease in the order of the main multipole contributions compared to the case in figure 19 indicates an increase in the radiative losses of symmetric states [see figure 17(b)].

3.8 Far-field two-photon amplitude

In the previous sections, we modeled radiation patterns and their multipole expansion for singly excited, high-Q states with $m = 1$ and $m = 2$. Recall that the most subradiant doubly excited state with $m = 3$ is a product of these singly excited states [according to figure 16]. In this section, we study the radiative directivity of the doubly excited state $|\Psi_1^{(3)}\rangle$.

For the doubly excited state, instead of the radiated power $|\Psi\rangle$, we will calculate a spatial two-photon amplitude [22]:

$$g_2(\mathbf{r}_a, \mathbf{r}_b) = \frac{\sum_{\alpha, \beta} \langle \Psi | \hat{E}_\beta(\mathbf{r}_b) \hat{E}_\alpha(\mathbf{r}_a) \hat{E}_\alpha^\dagger(\mathbf{r}_a) \hat{E}_\beta^\dagger(\mathbf{r}_b) | \Psi \rangle}{\sum_{\alpha, \beta} \langle \Psi | \hat{E}_\beta(\mathbf{r}_b) \hat{E}_\beta^\dagger(\mathbf{r}_b) | \Psi \rangle \langle \Psi | \hat{E}_\alpha(\mathbf{r}_a) \hat{E}_\alpha^\dagger(\mathbf{r}_a) | \Psi \rangle}, \quad (64)$$

where $\{\alpha, \beta\} = \{x, y, z\}$, $E_\alpha(\mathbf{r})$ is the electric field operator (1) creating a photon at point \mathbf{r} with polarization in α -direction, \mathbf{r}_a and \mathbf{r}_b are the coordinates of two detectors [see figure 21(a)]. The electric field operator is calculated using the far field Green's function (56), therefore, in the far field limit $r \gg \lambda_0$, equation (64) does not depend on $|\mathbf{r}_a|$, $|\mathbf{r}_b|$ upon the normalization.

Figure 21 shows two-photon amplitude (64) of high-Q state with $m = 3$ for two geometries of detectors. In the first case of figures 21(a,b), both detectors are placed at the same point and revolve around the rings. In the second one of figures 21(c,d), one of the detectors is fixed above the rings while the second one revolves. From the comparison of figures 21(b) and 21(d), we can conclude that the highest probability is the emission of photons in the same direction of $\theta \approx 75^\circ$ and $\varphi = 30^\circ, 90^\circ, 150^\circ, 210^\circ, 270^\circ, 330^\circ$ rather than in different directions. For these angles, the two-photon amplitude $g_2 > 1$ so demonstrates bunching.

In this chapter, we presented a mechanism that allows us to achieve the higher quality factors of singly and doubly excited states with angular quasi-momentum compared to the quality factors of the states in a single ring. We considered oligomers of quantum emitters supporting two singly excited states with

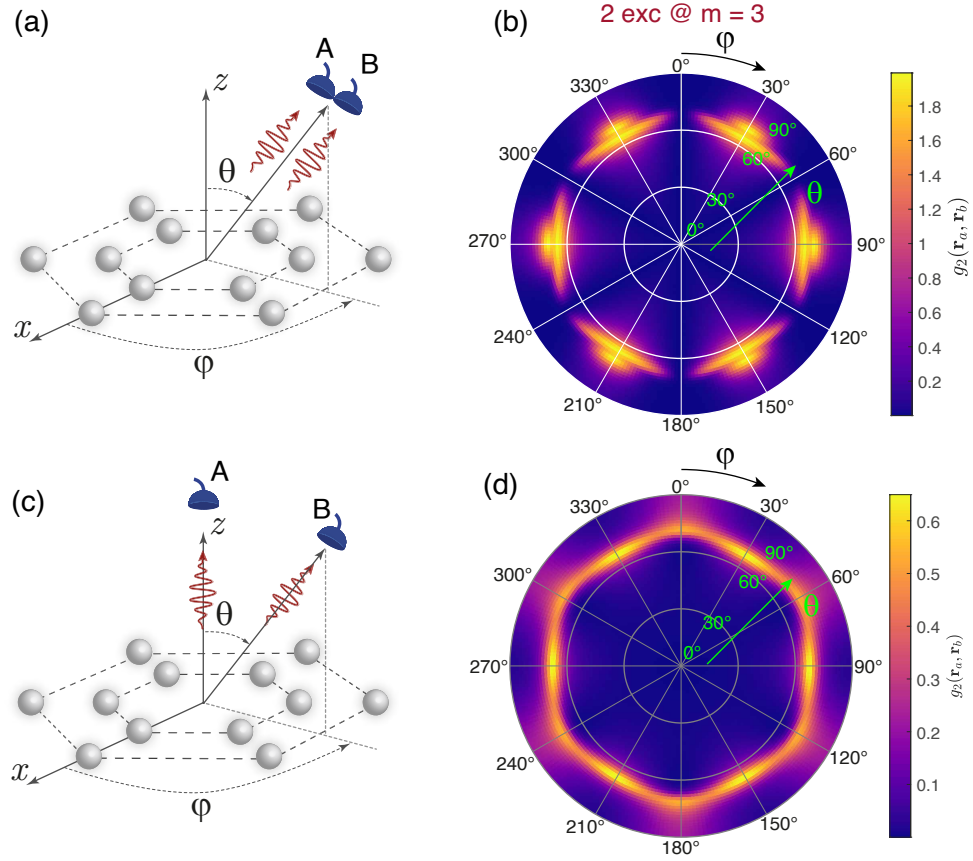


Figure 21 – (a,c) Detection schemes of two-photon emission for high-Q doubly excited state $|\Psi_1^{(3)}\rangle$ in figure 16(a). (b,d) The calculated two-photon far field amplitude (64) for detection schemes (a) and (c), respectively. In diagrams (b) and (d), θ angle is plotted along the radial direction and φ is along the angular direction. Note that the radiation patterns are symmetric with respect to the exchange $\theta \rightarrow \pi - \theta$ since the structures are placed in the xy plane

the same symmetry supported by subsystems of the oligomer. By optimizing the parameters of the oligomer, we achieve a regime of destructive interference between the states when the phase shift between them is close to π . In this regime, we observed maxima of the quality factors of singly excited states with $m = 0$ in the ring with a central emitter, and with all m in two concentric rings. It was shown that the high-Q states with angular quasi-momentum allow not only modifying far-field radiation patterns but also localizing and enhancing the transverse near fields. We performed the multipole expansion of far-field radiation of high-Q states in two rings and demonstrated that a high Q-factor is justified by the cancellation of low-order radiating multipole contributions due to the destructive interference between the rings. In the constructive interference regime, on the contrary, low-order multipoles dominate in the far field.

We showed that two rings of six emitters support not only high-Q singly excited states but also high-Q doubly excited states. We focused on the four doubly excited states with $m = 3$ and entering B_1 irreducible representation of C_{6v} symmetry group. This irreducible representation enters only the product of irreducible representations E_1 and E_2 of singly excited states with $m = \pm 1$ and $m = \pm 2$. Therefore, the energies of these doubly excited states with $m = 3$ are sums of energies of singly excited states with $m = \pm 1$ and $m = \pm 2$. Hence, there is a doubly excited state with $m = 3$ such that its energy is the sum of energies of high-Q states with $m = \pm 1$ and $m = \pm 2$. We found the optimal ring parameters such that the doubly excited state with $m = 3$ and singly excited states with $m = \pm 1$ and $m = \pm 2$ simultaneously have the maxima of Q-factors. We calculated the two-photon far-field amplitude of this doubly excited state and showed that this state demonstrates bunching in certain directions for the symmetric detection configuration.

CONCLUSION

In this thesis, we investigated subradiant (high-Q) singly and doubly excited states in quantum emitter ensembles (oligomers) with in-plane rotational symmetry. We clarified the mechanism of the formation of high-Q singly and doubly excited states with angular quasi-momentum m . This mechanism is based on the destructive interference of subsystems of emitter coupled via propagating photons in free space. The basic properties of these states were investigated. The main results of the work are highlighted below:

- a) We formulated the effective equations that allow us to find singly and doubly excited eigenstates in the system of concentric rings of emitters for each m .
- b) We derived the number of doubly excited eigenstates in the system of concentric rings of emitters for each m .
- c) We showed which irreducible representations of the symmetry C_{6v} group include singly excited states of a ring of six emitters.
- d) The selection rule for contributions of products of singly excited states into a doubly excited state is formulated: the irreducible representation of the doubly excited state should enter the product of irreducible representations of singly excited states.
- e) To achieve subradiant states, we consider oligomers that can be viewed as comprising two subsystems of emitters. The interaction between subsystems' states possessing the same symmetry (having the same m in our case) results in the formation of symmetric and anti-symmetric states, which also retain the initial states' symmetry. The anti-symmetric state has a large Q-factor compared to that of a single emitter for separations between emitters $a/\lambda_0 \lesssim 0.25$ because the phase shift between excitation amplitudes of subsystems is close to π leading to the suppression of low-order multipole contributions into the far-field radiation. It is shown that a ring with a central emitter supports a high-Q singly excited state with $m = 0$ ($Q_{\max}/Q_0 \sim 10^2$). Moreover, two concentric rings with the same number of emitters support high-Q singly excited states with all values of m possible for one ring ($Q_{\max}/Q_0 \sim 10^2 - 10^4$). In the high-Q state, an excitation occupies an inner subsystem, whereas, in the low-Q state, it occupies an outer subsystem.
- f) Two rings of six emitters support ten states with angular quasi-momentum $m = 3$ where four states enter the irreducible representation B_1 of the sym-

metry group C_{6v} . These states are pairs of excitations with $m = 1$ and $m = 2$ (or $m = -1$ and $m = -2$) being in the symmetric or anti-symmetric states. It was shown that the energies of these doubly excited states are the sums of energies of singly excited states with $m = 1$ and $m = 2$ (or $m = -1$ and $m = -2$). If both excitations are in the anti-symmetric states and have maxima of their Q-factors for certain parameters of the rings, the doubly excited state also has a maximum of the Q-factor for these parameters. Moreover, this state is the most subradiant doubly excited state in two rings ($Q_{\max}/Q_0 \sim 10^2$). In the high-Q doubly excited state, two excitations mainly occupy the inner ring of emitters.

REFERENCES

- 1 Solntsev A. S., Agarwal G. S., Kivshar Y. S. Metasurfaces for quantum photonics // *Nat. Photonics*. — 2021. — Vol. 15. — P. 327–336. — ISSN 1749-4893. — DOI: 10.1038/s41566-021-00793-z. — URL: <https://doi.org/10.1038/s41566-021-00793-z>.
- 2 Colloquium: Quantum matter built from nanoscopic lattices of atoms and photons / D. E. Chang [et al.] // *Rev. Mod. Phys.* — 2018. — Vol. 90, no. 3. — P. 031002. — ISSN 1539-0756. — DOI: 10.1103/RevModPhys.90.031002. — URL: <https://doi.org/10.1103/RevModPhys.90.031002>.
- 3 Facchinetti G., Jenkins S. D., Ruostekoski J. Storing Light with Subradiant Correlations in Arrays of Atoms // *Phys. Rev. Lett.* — 2016. — Vol. 117, no. 24. — P. 243601. — ISSN 1079-7114. — DOI: 10.1103/PhysRevLett.117.243601. — URL: <https://doi.org/10.1103/PhysRevLett.117.243601>.
- 4 Kalachev A. A., Samartsev V. V. Quantum memory and quantum computations in the optical subradiance regime // *Quantum Electron.* — 2005. — Vol. 35, no. 8. — P. 679. — ISSN 1063-7818. — DOI: 10.1070/QE2005v035n08ABEH010261. — URL: <https://doi.org/10.1070/QE2005v035n08ABEH010261>.
- 5 Parallel Implementation of High-Fidelity Multiqubit Gates with Neutral Atoms / H. Levine [et al.] // *Phys. Rev. Lett.* — 2019. — Vol. 123, no. 17. — P. 170503. — ISSN 1079-7114. — DOI: 10.1103/PhysRevLett.123.170503. — URL: <https://doi.org/10.1103/PhysRevLett.123.170503>.
- 6 Scully M., Zubairy M. *Quantum Optics*. — Cambridge University Press, Cambridge, UK, 1997.
- 7 Dicke R. H. Coherence in Spontaneous Radiation Processes // *Phys. Rev.* — 1954. — Vol. 93, no. 1. — P. 99–110. — ISSN 1536-6065. — DOI: 10.1103/PhysRev.93.99. — URL: <https://doi.org/10.1103/PhysRev.93.99>.
- 8 Freedhoff H., Van Kranendonk J. THEORY OF COHERENT RESONANT ABSORPTION AND EMISSION AT INFRARED AND OPTICAL FREQUENCIES // *Can. J. Phys.* — 1967. — DOI: 10.1139/p67-14.

- 9 Superradiant Effects in Systems of Two-Level Atoms / C. R. Stroud [et al.] // *Phys. Rev. A.* — 1972. — Vol. 5, no. 3. — P. 1094–1104. — ISSN 2469-9934. — DOI: 10 . 1103 / PhysRevA . 5 . 1094. — URL: <https://doi.org/10.1103/PhysRevA.5.1094>.
- 10 Experimental Evidence for Subradiance / D. Pavolini [et al.] // *Phys. Rev. Lett.* — 1985. — Vol. 54, no. 17. — P. 1917–1920. — ISSN 1079-7114. — DOI: 10.1103/PhysRevLett.54.1917. — URL: <https://doi.org/10.1103/PhysRevLett.54.1917>.
- 11 DeVoe R. G., Brewer R. G. Observation of Superradiant and Subradiant Spontaneous Emission of Two Trapped Ions // *Phys. Rev. Lett.* — 1996. — Vol. 76, no. 12. — P. 2049–2052. — ISSN 1079-7114. — DOI: 10.1103/PhysRevLett.76.2049. — URL: <https://doi.org/10.1103/PhysRevLett.76.2049>.
- 12 Nanometer Resolution and Coherent Optical Dipole Coupling of Two Individual Molecules / C. Hettich [et al.] // *Science.* — 2002. — Vol. 298, no. 5592. — P. 385–389. — ISSN 0036-8075. — DOI: 10 . 1126 / science . 1075606. — URL: <https://doi.org/10.1126/science.1075606>.
- 13 Guerin W., Arajo M. O., Kaiser R. Subradiance in a Large Cloud of Cold Atoms // *Phys. Rev. Lett.* — 2016. — Vol. 116, no. 8. — P. 083601. — ISSN 1079-7114. — DOI: 10 . 1103 / PhysRevLett . 116 . 083601. — URL: <https://doi.org/10.1103/PhysRevLett.116.083601>.
- 14 Atom-by-atom assembly of defect-free one-dimensional cold atom arrays / M. Endres [et al.] // *Science.* — 2016. — Vol. 354, no. 6315. — P. 1024–1027. — ISSN 0036-8075. — DOI: 10 . 1126 / science . aah3752. — URL: <https://doi.org/10.1126/science.aah3752>.
- 15 Defect-Free Assembly of 2D Clusters of More Than 100 Single-Atom Quantum Systems / D. Ohl de Mello [et al.] // *Phys. Rev. Lett.* — 2019. — Vol. 122, no. 20. — P. 203601. — ISSN 1079-7114. — DOI: 10 . 1103 / PhysRevLett.122.203601. — URL: <https://doi.org/10.1103/PhysRevLett.122.203601>.
- 16 An atom-by-atom assembler of defect-free arbitrary two-dimensional atomic arrays / D. Barredo [et al.] // *Science.* — 2016. — Vol. 354, no.

6315. — P. 1021–1023. — ISSN 0036-8075. — DOI: 10 . 1126 / science . aah3778. — URL: <https://doi.org/10.1126/science.aah3778>.
- 17 Synthetic three-dimensional atomic structures assembled atom by atom / D. Barredo [et al.] // *Nature*. — 2018. — Vol. 561. — P. 79–82. — ISSN 1476-4687. — DOI: 10 . 1038 / s41586 - 018 - 0450 - 2. — URL: <https://doi.org/10.1038/s41586-018-0450-2>.
 - 18 Sutherland R. T., Robicheaux F. Collective dipole-dipole interactions in an atomic array // *Phys. Rev. A*. — 2016. — Vol. 94, no. 1. — P. 013847. — ISSN 2469-9934. — DOI: 10 . 1103 / PhysRevA . 94 . 013847. — URL: <https://doi.org/10.1103/PhysRevA.94.013847>.
 - 19 Extremely subradiant states in a periodic one-dimensional atomic array / D. F. Kornovan [et al.] // *Phys. Rev. A*. — 2019. — Vol. 100, no. 6. — P. 063832. — ISSN 2469-9934. — DOI: 10 . 1103 / PhysRevA . 100 . 063832. — URL: <https://doi.org/10.1103/PhysRevA.100.063832>.
 - 20 Zhang Y.-X., Yu C., Mølmer K. Subradiant bound dimer excited states of emitter chains coupled to a one dimensional waveguide // *Phys. Rev. Res.* — 2020. — Vol. 2, no. 1. — P. 013173. — ISSN 2643-1564. — DOI: 10 . 1103 / PhysRevResearch . 2 . 013173. — URL: <https://doi.org/10.1103/PhysRevResearch.2.013173>.
 - 21 Poddubny A. N. Quasiflat band enabling subradiant two-photon bound states // *Phys. Rev. A*. — 2020. — Vol. 101, no. 4. — P. 043845. — ISSN 2469-9934. — DOI: 10 . 1103 / PhysRevA . 101 . 043845. — URL: <https://doi.org/10.1103/PhysRevA.101.043845>.
 - 22 Holzinger R., Moreno-Cardoner M., Ritsch H. Nanoscale continuous quantum light sources based on driven dipole emitter arrays // *Appl. Phys. Lett.* — 2021. — Vol. 119, no. 2. — ISSN 0003-6951. — DOI: 10.1063/5.0049270. — URL: <https://doi.org/10.1063/5.0049270>.
 - 23 High-Q Localized States in Finite Arrays of Subwavelength Resonators / D. F. Kornovan [et al.] // *ACS Photonics*. — 2021. — Vol. 8, no. 12. — P. 3627–3632. — DOI: 10 . 1021 / acsphotonics . 1c01262. — URL: <https://doi.org/10.1021/acsphotonics.1c01262>.

- 24 Bettles R. J., Gardiner S. A., Adams C. S. Cooperative ordering in lattices of interacting two-level dipoles // *Phys. Rev. A.* — 2015. — Vol. 92, no. 6. — P. 063822. — ISSN 2469-9934. — DOI: 10.1103/PhysRevA.92.063822. — URL: <https://doi.org/10.1103/PhysRevA.92.063822>.
- 25 Exponential Improvement in Photon Storage Fidelities Using Subradiance and “Selective Radiance” in Atomic Arrays / A. Asenjo-Garcia [et al.] // *Phys. Rev. X.* — 2017. — Vol. 7, no. 3. — P. 031024. — ISSN 2160-3308. — DOI: 10.1103/PhysRevX.7.031024. — URL: <https://doi.org/10.1103/PhysRevX.7.031024>.
- 26 Freedhoff H. S. Spontaneous emission by a fully excited system of three identical atoms // *J. Phys. B: At. Mol. Phys.* — 1986. — Vol. 19, no. 19. — P. 3035. — ISSN 0022-3700. — DOI: 10.1088/0022-3700/19/19/017. — URL: <https://doi.org/10.1088/0022-3700/19/19/017>.
- 27 Freedhoff H. S. Cooperative single-quantum excitations of a closed-ring polymer chain // *J. Chem. Phys.* — 1986. — Vol. 85, no. 10. — P. 6110–6117. — ISSN 0021-9606. — DOI: 10.1063/1.451476. — URL: <https://doi.org/10.1063/1.451476>.
- 28 Buck J. R., Kimble H. J. Optimal sizes of dielectric microspheres for cavity QED with strong coupling // *Phys. Rev. A.* — 2003. — Vol. 67, no. 3. — P. 033806. — ISSN 2469-9934. — DOI: 10.1103/PhysRevA.67.033806. — URL: <https://doi.org/10.1103/PhysRevA.67.033806>.
- 29 Polarization control of radiation and energy flow in dipole-coupled nanorings / J. Cremer [et al.] // *New J. Phys.* — 2020. — Vol. 22, no. 8. — P. 083052. — ISSN 1367-2630. — DOI: 10.1088/1367-2630/aba4d4. — URL: <https://doi.org/10.1088/1367-2630/aba4d4>.
- 30 Efficient nano-photonic antennas based on dark states in quantum emitter rings / M. Moreno-Cardoner [et al.] // *Opt. Express.* — 2022. — Vol. 30, no. 7. — P. 10779–10791. — ISSN 1094-4087. — DOI: 10.1364/OE.437396. — URL: <https://doi.org/10.1364/OE.437396>.
- 31 Nanoscale Coherent Light Source / R. Holzinger [et al.] // *Phys. Rev. Lett.* — 2020. — Vol. 124, no. 25. — P. 253603. — ISSN 1079-7114. — DOI: 10.1103/PhysRevLett.124.253603. — URL: <https://doi.org/10.1103/PhysRevLett.124.253603>.

- 32 Jen H. H., Chang M.-S., Chen Y.-C. Cooperative light scattering from helical-phase-imprinted atomic rings // *Sci. Rep.* — 2018. — Vol. 8, no. 9570. — P. 1–12. — ISSN 2045-2322. — DOI: 10 . 1038 / s41598 - 018 - 27888-y. — URL: <https://doi.org/10.1038/s41598-018-27888-y>.
- 33 Subradiance-enhanced excitation transfer between dipole-coupled nanorings of quantum emitters / M. Moreno-Cardoner [et al.] // *Phys. Rev. A.* — 2019. — Vol. 100, no. 2. — P. 023806. — ISSN 2469-9934. — DOI: 10 . 1103 / PhysRevA . 100 . 023806. — URL: <https://doi.org/10.1103/PhysRevA.100.023806>.
- 34 Volya A., Zelevinsky V. Non-Hermitian effective Hamiltonian and continuum shell model // *Phys. Rev. C.* — 2003. — Vol. 67, no. 5. — P. 054322. — ISSN 2469-9993. — DOI: 10 . 1103 / PhysRevC . 67 . 054322. — URL: <https://doi.org/10.1103/PhysRevC.67.054322>.
- 35 Bound states in the continuum / C. W. Hsu [et al.] // *Nat. Rev. Mater.* — 2016. — Vol. 1. — P. 16048. — ISSN 2058-8437. — DOI: 10 . 1038 / natrevmats.2016.48. — URL: <https://doi.org/10.1038/natrevmats.2016.48>.
- 36 Radial bound states in the continuum for polarization-invariant nanophotonics / L. Khner [et al.] // *Nat. Commun.* — 2022. — Vol. 13, no. 4992. — P. 1–8. — ISSN 2041-1723. — DOI: 10 . 1038 / s41467 - 022 - 32697-z. — URL: <https://doi.org/10.1038/s41467-022-32697-z>.
- 37 Bound states in the continuum in photonic structures / K. L. Koshelev [et al.] // *Phys.-Usp.* — 2023. — Vol. 66, no. 5. — ISSN 1063-7869. — URL: <https://ufn.ru/en/articles/2023/5/c>.
- 38 Breuer H. P., Petruccione F. *The Theory of Open Quantum Systems.* — Oxford University Press, 2002.
- 39 Gardiner C., Zoller P. *Quantum Noise: a Handbook of Markovian and non-Markovian Quantum Stochastic Methods with Applications to Quantum Optics.* — Springer Science & Business Media, Berlin/Heidelberg, Germany, 2004.
- 40 Tavis M., Cummings F. W. Exact Solution for an N -Molecule—Radiation-Field Hamiltonian // *Phys. Rev.* — 1968. — Vol. 170, no. 2.

- P. 379–384. — ISSN 1536-6065. — DOI: 10.1103/PhysRev.170.379.
— URL: <https://doi.org/10.1103/PhysRev.170.379>.
- 41 Lehmberg R. H. Radiation from an N -Atom System. I. General Formalism // Phys. Rev. A. — 1970. — Vol. 2, no. 3. — P. 883–888. — ISSN 2469-9934. — DOI: 10.1103/PhysRevA.2.883. — URL: <https://doi.org/10.1103/PhysRevA.2.883>.
- 42 Dung H. T., Knll L., Welsch D.-G. Resonant dipole-dipole interaction in the presence of dispersing and absorbing surroundings // Phys. Rev. A. — 2002. — Vol. 66, no. 6. — P. 063810. — ISSN 2469-9934. — DOI: 10.1103/PhysRevA.66.063810. — URL: <https://doi.org/10.1103/PhysRevA.66.063810>.
- 43 Breuer H.-P., Petruccione F. The Theory of Open Quantum Systems. — 2006. — ISBN 978-0-19921390-0. — DOI: 10.1093/acprof:oso/9780199213900.001.0001. — URL: <https://doi.org/10.1093/acprof:oso/9780199213900.001.0001>.
- 44 Novotny L., Hecht B. Principles of Nano-Optics. — Cambridge University Press, 2006. — DOI: 10.1017/CBO9780511813535.
- 45 Optical response features of Si-nanoparticle arrays / A. B. Evlyukhin [et al.] // Phys. Rev. B. — 2010. — Vol. 82, no. 4. — P. 045404. — ISSN 2469-9969. — DOI: 10.1103/PhysRevB.82.045404. — URL: <https://doi.org/10.1103/PhysRevB.82.045404>.
- 46 Vries P. de, Coevorden D. V. van, Lagendijk A. Point scatterers for classical waves // Rev. Mod. Phys. — 1998. — Vol. 70, no. 2. — P. 447–466. — ISSN 1539-0756. — DOI: 10.1103/RevModPhys.70.447. — URL: <https://doi.org/10.1103/RevModPhys.70.447>.
- 47 Gangaraj S. A. H., Hanson G. W., Antezza M. Robust entanglement with three-dimensional nonreciprocal photonic topological insulators // Phys. Rev. A. — 2017. — Vol. 95, no. 6. — P. 063807. — ISSN 2469-9934. — DOI: 10.1103/PhysRevA.95.063807. — URL: <https://doi.org/10.1103/PhysRevA.95.063807>.
- 48 Chew W. C. Waves and Fields in Inhomogenous Media. — Wiley-IEEE Press, 1995. — URL: <https://ieeexplore.ieee.org/book/5270998>.

- 49 Bohren C. F., Huffman D. R. Absorption and Scattering of Light by Small Particles. — 1998. — ISBN 978-0-47129340-8. — DOI: 10 . 1002 / 9783527618156. — URL: <https://doi.org/10.1002/9783527618156>.